MID-AMERICA
TRANSPORTATION CENTER

Report # MATC-UNL: 427

Final Report

Impact of Truck Loading on Design and Analysis of Asphaltic Pavement Structures-Phase III

Yong-Rak Kim, Ph.D.
Associate Professor
Department of Civil Engineering
University of Nebraska-Lincoln

Hoki Ban, Ph.D.
Postdoctoral Research Associate

Soohyok Im
Ph.D. Candidate

2012

A Cooperative Research Project sponsored by the U.S. Department of Transportation Research and Innovative Technology Administration

Impact of Truck Loading on Design and Analysis of Asphaltic Pavement Structures-Phase III

Yong-Rak Kim, Ph.D.
Associate Professor
Department of Civil Engineering
University of Nebraska-Lincoln

Hoki Ban, Ph.D.
Postdoctoral Research Associate
Department of Civil Engineering
University of Nebraska-Lincoln

Soohyok Im
Ph.D. Candidate
Department of Civil Engineering
University of Nebraska-Lincoln

A Report on Research Sponsored by

Mid-America Transportation Center

University of Nebraska-Lincoln

March 2012

Technical Report Documentation Page

1. Report No. 25-1121-0001-427	2. Government Accession No.	3. Recipient's Catalog No.
4. Title and Subtitle Impact of Truck Loading on Design and Analysis of Asphaltic Pavement Structures-Phase III		5. Report Date March 2012 6. Performing Organization Code
7. Author(s) Soohyok Im, Hoki Ban, and Yong-Rak Kim		8. Performing Organization Report No. 25-1121-0001-427
9. Performing Organization Name and Address Mid-America Transportation Center 2200 Vine St. PO Box 830851 Lincoln, NE 68583-0851		10. Work Unit No. (TRAIS) 11. Contract or Grant No.
12. Sponsoring Agency Name and Address Research and Innovative Technology Administration 1200 New Jersey Ave., SE Washington, D.C. 20590		13. Type of Report and Period Covered Final Report July 2010-March 2012 14. Sponsoring Agency Code MATC TRB RiP No. 28480
15. Supplementary Notes		

16. Abstract

This study investigated the impact of the realistic constitutive material behavior of asphalt layer (both nonlinear inelastic and fracture) for the prediction of pavement performance. To this end, this study utilized a cohesive zone model to consider the fracture behavior of asphalt mixtures at an intermediate temperature condition. The semi-circular bend (SCB) fracture test was conducted to characterize the fracture properties of asphalt mixtures. Fracture properties were then used to simulate mechanical responses of pavement structures. In addition, Schapery's nonlinear viscoelastic constitutive model was implemented into the commercial finite element software ABAQUS via a user defined subroutine (user material, or UMAT) to analyze asphalt pavement subjected to heavy truck loads. Extensive creep-recovery tests were conducted at various stress levels and multiple service temperatures to obtain the stress- and temperature-dependent viscoelastic material properties of asphalt mixtures. Utilizing the derived viscoelastic and fracture properties and the UMAT code, a typical pavement structure was modeled that simulated the effect of material nonlinearity and damage due to repeated heavy truck loads. Two-dimensional finite element simulations of the pavement structure demonstrated significant differences between the cases: linear viscoelastic and nonlinear viscoelastic modeling with and without fracture in the prediction of pavement performance. The differences between the cases were considered significant, and should be addressed during the process of performance-based pavement design. This research demonstrates the importance of accurate and more realistic characterizations of pavement materials.

17. Key Words Asphalt pavement, performance modeling, nonlinear viscoelasticity, fracture, finite element method	18. Distribution Statement		
19. Security Classif. (of this report) Unclassified	20. Security Classif. (of this page) Unclassified	21. No. of Pages 57	22. Price

Table of Contents

List of Figures

List of Tables

List of Abbreviations

Bituminous Foundation Course (BFC)
Digital Image Correlation (DIC)
Fracture Process Zone (FPZ)
Linear Elastic Fracture Mechanics (LEFM)
Linear Variable Differential Transformers (LVDT)
Mechanistic-Empirical (M-E)
Mechanistic-Empirical Pavement Design Guide (MEPDG)
Notch Mouth Opening Displacements (NMOD)
Notch Tip Opening Displacements (NTOD)
Portland cement concrete (PCC)
Semi-Circular Bend (SCB)
User Material (UMAT)

Acknowledgments

The authors would like to thank the Mid-America Transportation Center (MATC) for providing the financial support necessary to complete this study.

Disclaimer

The contents of this report reflect the views of the authors, who are responsible for the facts and the accuracy of the information presented herein. This document is disseminated under the sponsorship of the Department of Transportation University Transportation Centers Program, in the interest of information exchange. The U.S. Government assumes no liability for the contents or use thereof.

Abstract

This study investigated the impact of the realistic constitutive material behavior of asphalt layer (both nonlinear inelastic and fracture) for the prediction of pavement performance. To this end, this study utilized a cohesive zone model to consider the fracture behavior of asphalt mixtures at an intermediate temperature condition. The semi-circular bend (SCB) fracture test was conducted to characterize the fracture properties of asphalt mixtures. Fracture properties were then used to simulate mechanical responses of pavement structures. In addition, Schapery's nonlinear viscoelastic constitutive model was implemented into the commercial finite element software ABAQUS via a user defined subroutine (user material, or UMAT) to analyze asphalt pavement subjected to heavy truck loads. Extensive creep-recovery tests were conducted at various stress levels and multiple service temperatures to obtain the stress- and temperature-dependent viscoelastic material properties of asphalt mixtures. Utilizing the derived viscoelastic and fracture properties and the UMAT code, a typical pavement structure was modeled that simulated the effect of material nonlinearity and damage due to repeated heavy truck loads. Two-dimensional finite element simulations of the pavement structure demonstrated significant differences between the cases: linear viscoelastic and nonlinear viscoelastic modeling with and without fracture in the prediction of pavement performance. The differences between the cases were considered significant, and should be addressed during the process of performance-based pavement design. This research demonstrates the importance of accurate and more realistic characterizations of pavement materials.

Chapter 1 Introduction

Distresses in asphalt pavements, such as rutting and fatigue cracking, are critical safety issues affecting roadway users. Rutting, or, permanent deformation, is surface depression resulting from the accumulation of vertical displacements in asphalt pavement layers. The presence of this distress is even more dangerous for roadway users when the surface depression is filled with water. Accumulation of water in surface depressions increases the risk of vehicle hydroplaning, and, as a result of freezing and thawing cycles in cold regions, weakens pavement layers. Large damage areas, such as potholes, result from severe fatigue cracking in the pavement, combined with thermal stress. Pavement design methods should account for the combination of multiple factors that cause these distresses (i.e., traffic loads, environmental effects, and composite material constituent's combinations and interactions), in order to improve the reliability of the structures.

A few approaches have been adopted by the research community to examine the effects of these distress-causing factors on pavement response. Conventional asphalt pavement design methods assume that asphalt layers are made of materials with linear-elastic response; however, asphaltic materials exhibit viscoelastic material behavior that is significantly affected by the rate of loading, time, and temperature conditions. It has been observed that results from elastic analyses do not correlate well with field measurements. To improve the accuracy of these analyses, many studies have adopted the viscoelastic constitutive model to predict the behavior of asphaltic materials (Al-Qadi et al. 2005; Elseifi et al. 2006; Yoo 2007; Kim et al. 2008; Kim et al. 2009). However, nonlinear response was not taken into consideration in these models in spite of abundant experimental observations (Masad and Somadevan 2002; Collop et al. 2003; Airey et al. 2004) that present nonlinear response of asphalt binders and mixes at certain levels of stress

and strain. Therefore, it is necessary to consider stress-dependent nonlinear viscoelastic material characteristics at various stress levels.

To this end, this study characterized the nonlinear viscoelastic behavior of asphalt mixtures using Schapery's nonlinear viscoelastic model. The model was implemented into the commercial finite element software ABAQUS as a user-defined subroutine, labeled UMAT (user material) based on the recursive-iterative numerical algorithm determined by Haji-Ali and Muliana (2004). Extensive creep-recovery tests were conducted at various stress levels and at two temperatures (30^{o}C and 40^{o}C) in order to obtain the stress- and temperature-dependent nonlinear viscoelastic material properties of asphalt mixtures. Material properties were then used to simulate mechanical responses of pavement structures. Detailed investigations of the pavement responses resulting from different constitutive relations (such as linear viscoelastic and nonlinear viscoelastic) can provide better understanding of the effects of truck loading on pavement damage and consequently advance the current pavement analysis-design method.

The recent mechanistic-empirical (M-E) design guide predicts fatigue cracking resistance of asphalt pavements by considering various factors mentioned above. However, the M-E design guide is known to be limited in its ability to accurately predict mechanical responses in asphaltic pavements due to the use of empirically developed prediction models. Recently, the fracture behavior of asphalt mixtures has been studied by several researchers through fracture tests and numerical analysis by means of a cohesive zone model (Marasteanu et al. 2002; Wagoner et al. 2005, 2006; Kim et al. 2008). Most studies were conducted at low temperature conditions; however, since fracture behavior at intermediate service temperatures is sensitive to loading rates, this study considered the fracture behavior of asphalt mixtures at an intermediate temperature condition (30^{o}C) using the cohesive zone model. The SCB fracture test was

conducted to characterize the fracture properties of asphalt mixtures. Fracture properties were then used to simulate mechanical responses of pavement structures subjected to heavy truck loads.

1.1 Research Scope and Objective

The purpose of the current study was to provide a better understanding of the effects of heavy-load trucks on pavement performance. Trucking is the most dominant component of U.S. freight transportation, and is expected to grow significantly in the future. Better preservation of the existing highway infrastructure against heavy-load trucks is therefore a necessity. Success in this endeavor can be achieved through more accurate and realistic analyses of pavement structures.

For a more accurate and realistic analysis of pavement structures against heavy-load trucks, a series of research efforts led by the primary investigator was initiated in FY 2009 and continued in FY 2010. These efforts investigated pavement performance predictions from both the newly released "Mechanistic-Empirical Pavement Design Guide" (MEPDG) approach and the purely mechanistic approach based on the "Finite Element Method." The research particularly focused on the impact of heavy truck loads on pavement damage. Analysis results during FY 2009 and FY 2010 clearly demonstrated that both material inelasticity (e.g., the viscoelastic nature of asphaltic materials and elasto-plastic behavior of soils) and realistic tire loading configuration, which are not rigorously implemented in the current MEPDG, can mislead predictions of pavement rutting. These misled predictions can result in significant errors in the design of pavement structure as well as in the prediction of pavement performance when the empirical damage evolution relations in the MEPDG are further incorporated.

Based on research outcomes observed during FY 2009 and FY 2010, this study, "Phase III" extends the previous research scope to facilitate a more realistic analysis of pavement performance. In this study, a more detailed investigation of pavement responses was pursued by focusing on the fracture- (cracking) related damage behavior of pavement structures. Any significant differences between the cases were considered important factors that should be deliberately examined for a more precise implementation of pavement analysis and design in future research.

1.2 Organization of the Report

This report is composed of seven chapters. Following the current introduction, chapter 2 summarizes literature on rutting and cracking. Chapter 3 presents the theoretical background of Schapery's nonlinear viscoelastic constitutive model and its numerical implementation into a finite element code. The theoretical background of the cohesive zone model is also presented in chapter 3. Chapter 4 describes the creep-recovery test and the fracture test conducted to identify viscoelastic and fracture properties of asphalt mixtures. Chapter 5 describes how the viscoelastic and fracture properties were obtained from the laboratory test results. From the material properties identified in chapter 5, chapter 6 describes finite element simulations of a pavement structure, taking into account the effect of material viscoelasticity (linear and nonlinear) and fracture of pavement subjected to heavy truck loads. Simulation results and significant observations are discussed. Finally, chapter 7 summarizes this study and its conclusions.

Chapter 2 Literature Review

2.1 Studies on Rutting

Rutting is one of the primary distresses in flexible pavement systems. Rutting is caused by plastic or permanent deformation in the asphalt concrete, unbound layers, and foundation soils. The M-E design guide predicts rutting performance of flexible pavements by considering the constitutive relationship between predicted rutting in the asphalt mixture and field-calibrated statistical analyses of repeated load permanent deformation tests conducted in the laboratory. The laboratory-derived relationship is then adjusted to match the rut depth measured from the roadway (AASHTO 2008).

Although the M-E design guide employs various design parameters (climate, traffic, materials, etc.) to predict the performance of flexible pavements, it is known to be limited in its ability to accurately predict mechanical responses in asphaltic pavements due to the use of simplified structural analysis methods, a general lack of understanding of the fundamental constitutive behavior and damage mechanisms of paving materials, and the use of circular tire loading configurations.

To overcome the limitations of the layered elastic approaches, many researchers have attempted to develop structural mechanistic models that are able to predict the performance of asphaltic pavements. In order to represent the behavior of asphalt mixtures under different boundary conditions, it is necessary to incorporate constitutive material models into these structural mechanistic models. Computational approaches such as the finite element technique have received increased attention from the pavement mechanics community due to their extremely versatile implementation of mechanical characteristics in addressing complex issues such as inelastic constitutive behavior, irregular pavement geometry (Blab and Harvey 2002; Al-

Qadi et al. 2002; Collop et al. 2003; Al-Qadi et al. 2004; Al-Qadi et al. 2005), and growing damage (Mun et al. 2004; Elseifi and Al-Qadi 2006; Kim et al. 2006).

Recently, several studies (Al-Qadi et al. 2005; Elseifi et al. 2006; Kim et al., 2009) have conducted viscoelastic analyses that considered the asphalt layer as linear viscoelastic and the other layers as elastic, using the finite element method in two dimensional (2-D) or three-dimensional (3-D) models for predicting the time-dependent response of flexible pavement. However, nonlinear response was not taken into consideration in these models, in spite of abundant experimental observations (Masad and Somadevan 2002; Collop et al. 2003; Airey et al. 2004) that demonstrated nonlinear response of asphalt binders and mixes at certain levels of stress and strain. For example, figure 2.1, which presents test results from Masad and Somadevan (2002), illustrates that the nonlinearity is evident as the shear modulus decreases with an increase in strain level. For a linear material, the curves in the figure would coincide. Therefore, it is necessary to consider the nonlinear viscoelastic responses when asphalt pavements are subjected to heavy loads.

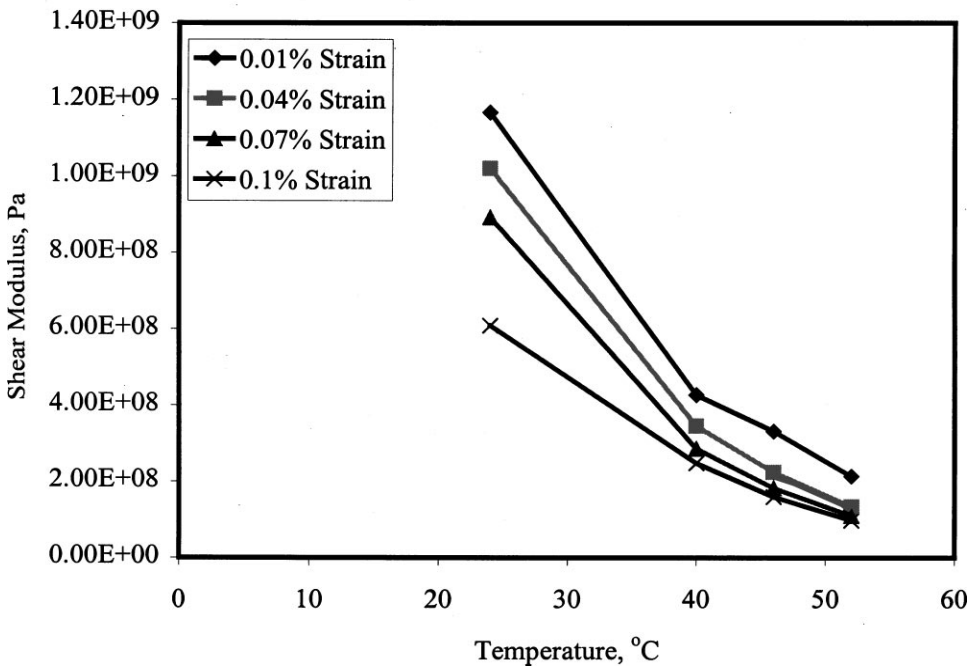

Figure 2.1 Test results from Masad and Somadevan (2002)

2.2 Studies on Cracking

Various asphalt pavement distresses are related to fracture including fatigue cracking (both top-down and bottom-up), thermal (transverse) cracking, and reflective cracking of the asphalt layer. Cracking in asphaltic pavement layers causes primary failure of the roadway structure and leads to long-term durability issues, and are often related to moisture damage. The fracture resistance and characteristics of asphalt materials significantly influence the service life of asphalt pavements and consequently the maintenance and management of the pavement network. In spite of its significant implications, proper characterization of the fracture process and fundamental fracture properties of the asphaltic materials have not been adopted in the current pavement design-analysis procedures which are generally phenomenological.

Cracking is probably the most challenging issue to predict and control. This is because of the complex geometric characteristics and inelastic mechanical behavior of the asphalt mixtures,

which are temperature sensitive and rate dependent. These characteristics make any solution to the cracking problem in asphalt mixtures almost impossible to achieve via the theory of linear elastic fracture mechanics (LEFM). LEFM is only able to predict the stress state close to the crack tips of damaged bodies if the fracture process zone (FPZ) around the crack tip is very small. The FPZ in asphaltic materials might be large, as is typical of quasi-brittle materials (Bazant and Planas 1998).

Some studies have evaluated the fracture toughness of asphalt mixtures using the J-integral concept or the stress intensity approach (Mobasher et al. 1997; Mull et al. 2002; Kim et al., 2003). Others have conducted fracture tests and numerical analyses by means of a cohesive zone model to study the fracture behavior of asphalt mixtures (Li and Marasteanu 2005; Song et al. 2006; Kim et al. 2007; Kim et al. 2009). The cohesive zone modeling approach has recently received increased attention from the asphaltic materials and pavement mechanics community for modeling crack initiation and growth. The cohesive zone approach can properly model both brittle and ductile fracture, which is frequently observed in asphaltic roadways due to the wide range of service temperatures and traffic speeds. Moreover, it can provide an efficient tool that can be easily implemented in various computational methods, such as finite element and discrete element methods, so that fracture events in extremely complicated mixture microstructure can also be simulated.

To monitor averaged deformations or displacements for the characterization of fracture properties of asphalt mixtures, most fracture tests have traditionally used conventional extensometers or clip-on gauges far from the actual FPZ. However, the true fracture properties of asphalt mixtures could be misled by as much as an order of magnitude, since the material responses captured by the extensometers or clip-on gauges are limited in their ability to

accurately represent material behavior at the actual FPZ. This discrepancy can worsen if the material is highly heterogeneous and inelastic (Song et al. 2008; Aragão 2011), which is typical in asphaltic paving materials. In addition, most of the studies have adopted low-temperature testing conditions in which the type of fracture is much more brittle and elastic. However, as shown in figure 2.2 (Aragão and Kim 2011), fracture behavior of asphaltic materials at intermediate service temperatures is sensitive to the loading rates. In order to accurately characterize intermediate temperature fracture behavior such as fatigue cracking, Aragão and Kim (2011) conducted fracture tests at 21^{o} C. Test results presented significant rate-dependent behavior.

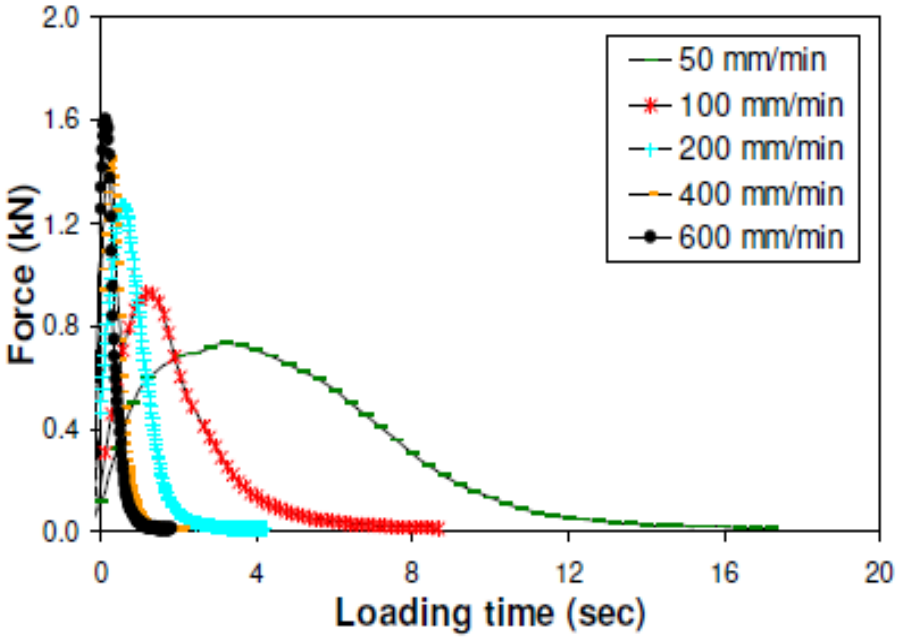

Figure 2.2 Fracture behavior at intermediate service temperatures

A better understanding of the FPZ at realistic service conditions is a critical step in the development of mechanistic design-analysis procedures for asphaltic mixtures and pavement

structures. This is because characteristics of the FPZ represent the true material behavior relative to fracture damage, which, consequently, leads to the selection of proper testing methods and modeling-analysis techniques that appropriately address the complex local fracture process. However, such careful efforts to characterize the FPZ in asphalt concrete mixtures have been, to date, insufficient. To our best knowledge, only limited attempts (Kim et al. 2002; Seo et al. 2002; Song et al. 2008; Li and Marasteanu 2010) have been carried out due to the many experimental-analytical complexities.

Chapter 3 Nonlinear Viscoelasticity and Cohesive Zone Model

The current chapter presents more advanced constitutive models for better characterization and performance prediction of asphalt mixtures. A multiaxial nonlinear viscoelastic constitutive model developed by Schapery (1969) is briefly introduced, and the numerical implementation incorporated with the finite element method is described. Schapery's single integral constitutive model was implemented into the commercial finite element software ABAQUS via a user-defined material called UMAT. In accordance with Schapery's model, the cohesive zone model was described to account for the fracture process as a gradual separation.

3.1 Schapery's Nonlinear Viscoelastic Model

Schapery's nonlinear viscoelastic single-integral constitutive model (Schapery 1969) for one-dimensional problems can be expressed in terms of an applied stress (σ) as follows:

$$\varepsilon(t) = g_0 D_0 \sigma + g_1 \int_0^t \Delta D\left[\psi(t) - \psi(\tau)\right] \frac{d\left(g_2 \sigma\right)}{d\tau} d\tau \tag{3.1}$$

where,

ψ is the reduced time given by:

$$\psi(t) = \int_0^t \frac{d\xi}{a_\sigma} \tag{3.2}$$

where,

g_0, g_1, g_2 and a_σ are the nonlinear viscoelastic parameters associated with stress level. These parameters are always positive and equal to 1 for the Boltzmann integral in linear viscoelasticity. It is noted that equation 3.2 can include not only stress effect, but also effects

such as temperature, moisture, and physical aging as each shift factor. D_0 and ΔD are uniaxial instantaneous and transient creep compliance at linear viscoelasticity respectively. The uniaxial transient compliance can be expressed in the form of a Prony series as:

$$\Delta D(\psi) = \sum_{n=1}^{N} D_n \left[1 - \exp\left(-\lambda_n \psi\right)\right] \tag{3.3}$$

where,

N is the number of Prony series, and D_n and λ_n are nth coefficient of the Prony series and the nth reciprocal of retardation time, respectively. Therefore equation 3.1 can be rewritten by substituting equation 3.3 into equation 3.1 as:

$$\varepsilon(t) = g_0 D_0 \sigma + g_1 g_2 \sum_{n=1}^{N} D_n - g_1 \sum_{n=1}^{N} D_n Q_n \tag{3.4}$$

where,

$$Q_n = \int_0^t \exp\left\{-\lambda_n \left[\psi(t) - \psi(\tau)\right]\right\} \frac{dg_2 \sigma}{d\tau} d\tau \tag{3.5}$$

The one-dimensional integral in equation 3.1 can be generalized to describe the multi-axial (i.e., 3-D) constitutive relations for an isotropic media by decoupling the response into deviatoric and volumetric strains as follows (Lai and Bakker 1996):

$$e_{ij}(t) = \frac{1}{2} g_0 J_0 S_{ij} + \frac{1}{2} g_1 \int_0^t \Delta J\left[\psi(t) - \psi(\tau)\right] \frac{d\left(g_2 S_{ij}\right)}{d\tau} d\tau \tag{3.6}$$

$$\varepsilon_{kk}(t) = \frac{1}{3} g_0 B_0 \sigma_{kk} + \frac{1}{3} g_1 \int_0^t \Delta B\left[\psi(t) - \psi(\tau)\right] \frac{d\left(g_2 \sigma_{kk}\right)}{d\tau} d\tau \tag{3.7}$$

where,

e_{ij}, ε_{kk}, and S_{ij} are deviatoric strain, volumetric strain, and deviatoric stress, respectively. J_0, B_0, ΔJ, and ΔB are the instantaneous and transient elastic shear and bulk compliance, respectively. The shear transient compliance $\Delta J(\psi)$ and the bulk transient compliance $\Delta B(\psi)$ can also be expressed by the Prony series as follows:

$$\Delta J(\psi) = \sum_{n=1}^{N} J_n \left[1 - \exp\left(-\lambda_n \psi\right)\right] \tag{3.8}$$

$$\Delta B(\psi) = \sum_{n=1}^{N} B_n \left[1 - \exp\left(-\lambda_n \psi\right)\right] \tag{3.9}$$

Assuming that Poisson's ratio υ is time-independent, the instantaneous and transient shear and bulk compliance can be evaluated from the following relations:

$$\begin{aligned} J_0 &= 2(1+\upsilon) D_0 \qquad B_0 = 3(1-2\upsilon) D_0 \\ \Delta J(\psi) &= 2(1+\upsilon) \Delta D(\psi) \qquad \Delta B(\psi) = 3(1-2\upsilon) \Delta D(\psi) \end{aligned} \tag{3.10}$$

The nonlinear parameters are assumed to be general polynomial functions of the effective shear stress $\bar{\sigma}$ which can be written as (Haji-Ali and Muliana 2004):

$$g_0 = 1 + \sum_{i=1}^{n} \alpha_i \left\langle \frac{\bar{\sigma}}{\sigma_0} - 1 \right\rangle^i, \quad g_1 = 1 + \sum_{i=1}^{n} \beta_i \left\langle \frac{\bar{\sigma}}{\sigma_0} - 1 \right\rangle^i$$
$$g_2 = 1 + \sum_{i=1}^{n} \gamma_i \left\langle \frac{\bar{\sigma}}{\sigma_0} - 1 \right\rangle^i, \quad a_\sigma = 1 + \sum_{i=1}^{n} \delta_i \left\langle \frac{\bar{\sigma}}{\sigma_0} - 1 \right\rangle^i \tag{3.11}$$

where,

$$\langle x \rangle = \begin{cases} x, & x > 0 \\ 0, & x \le 0 \end{cases}, \quad \bar{\sigma} = \sqrt{\frac{3}{2} S_{ij} S_{ij}}$$

The polynomial coefficients (α_i, β_i, γ_i, δ_i) can be calibrated from the creep and recovery tests at various stress levels. The term σ_0 is the effective shear stress limit in the linear viscoelastic range.

Next, the deviatoric and volumetric components can be expressed in terms of the hereditary integral formulation by substituting equation 3.8 into equation 3.6 and equation 3.9 into equation 3.7 as follows (Haji-Ali and Muliana 2004):

$$e_{ij}(t) = \frac{1}{2}\left[g_0 J_0 + g_1 g_2 \sum_{n=1}^{N} J_n \right] S_{ij} - \sum_{n=1}^{N} Q_{ij,n} \tag{3.12}$$

$$\varepsilon_{kk}(t) = \frac{1}{3}\left[g_0 B_0 + g_1 g_2 \sum_{n=1}^{N} B_n \right] \sigma_{kk} - \sum_{n=1}^{N} Q_{kk,n} \tag{3.13}$$

where,

$$Q_{ij,n} = \frac{1}{2} g_1 \int_0^t J_n \exp\left\{-\lambda_n \left[\psi(t) - \psi(\tau)\right]\right\} \frac{d\left(g_2 S_{ij}\right)}{d\tau} d\tau \tag{3.14}$$

$$Q_{kk,n} = \frac{1}{3} g_1 \int_0^t B_n \exp\left\{-\lambda_n \left[\psi(t) - \psi(\tau)\right]\right\} \frac{d\left(g_2 \sigma_{kk}\right)}{d\tau} d\tau \tag{3.15}$$

The derived 3-D nonlinear viscoelastic equations were numerically implemented into the well-known commercial finite element software ABAQUS via a user-defined material called UMAT, using the recursive integration scheme developed by Haj-Ali and Muliana (2004). In an attempt to verify whether the UMAT subroutine code was properly implemented in the finite element mainframe, one simple example problem was introduced. Code verification can be conducted simply by comparing computational results from the finite element code to analytical results obtained from the easily solvable problem. The example problem to be analyzed for code verification is shown in figure 3.1.

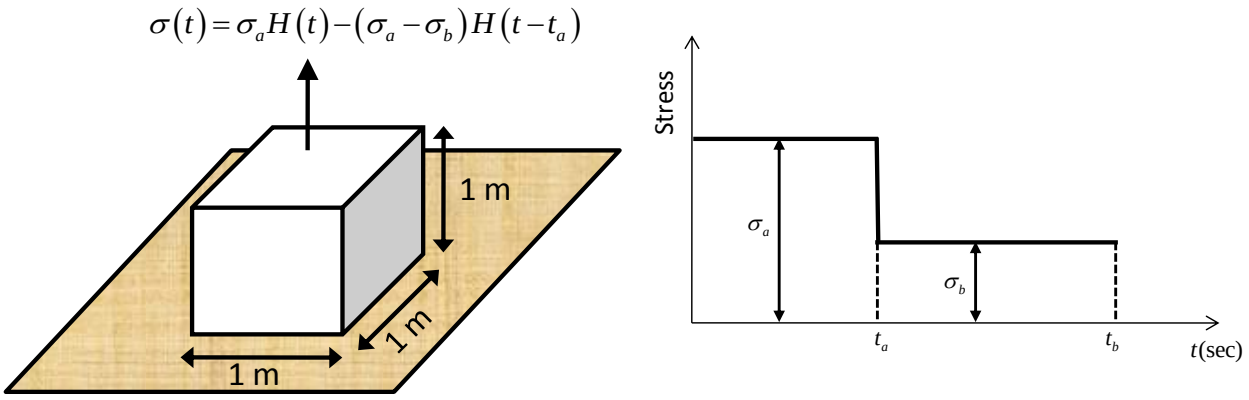

Figure 3.1 Example problem to verify UMAT code

Supposing a simple viscoelastic uniaxial bar is subjected to a two-step tensile load as presented in figure 3.1, the first loading of 1.0N is applied for 10 seconds, then reduced to 0.5N for 40 seconds. The resulting strain response can be derived as:

$$\varepsilon_c(t) = \left[g_0^a D_0 + g_1^a g_2^a D\left(\frac{t}{a_\sigma^a} \right) \right] \sigma_a \quad \text{for } 0 < t < t_a \tag{3.16}$$

$$\varepsilon_r(t) = g_0^b D_0 \sigma_b + g_1^b \left[g_2^a \sigma_a D\left(\frac{t_a}{a_\sigma^a} + \frac{t - t_a}{a_\sigma^b} \right) + \left(g_2^b \sigma_b - g_2^a \sigma_a \right) D\left(\frac{t - t_a}{a_\sigma^b} \right) \right] \quad \text{for } t_a < t < t_b$$

(3.17)

The creep compliance $D(t)$ is linear viscoelastic material property represented as the Prony series. Since this problem is merely for the sake of code verification, a simple form of the creep compliance is assumed as follows:

$$D(t) = D_0 + D_1 \left[1 - \exp(-\lambda t) \right] \tag{3.18}$$

where,

$$D_0 \equiv \frac{1}{E_0}, E_0 \equiv E_\infty + E_1, D_1 \equiv \frac{1}{E_\infty} - \frac{1}{E_0}, \ \lambda = \frac{E_\infty}{E_0} \cdot \frac{1}{\rho}$$

For the UMAT code verification, a special case of nonlinear viscoelastic response where $g_0 = g_1 = g_2 = a_\sigma = 1$ was first simulated. When the nonlinear viscoelastic model parameters are all equal to unity, the nonlinear viscoelastic model reduces to a linear viscoelastic hereditary integral. An analytical linear viscoelastic solution can then be calculated and compared to the computational results from the finite element analysis. Good agreement between the two results infers that the code was developed appropriately. As shown in figure 3.2, the linear viscoelastic finite element prediction and analytical solution match very well.

Secondly, in an attempt to examine the role of material nonlinearity in the model, the same uniaxial bar problem was simulated by assigning that the two parameters (g_0^a and a_σ^a) are equal to unity, while the other two nonlinear parameters are assumed as $g_1^a = g_2^a = 1.1$ during the first loading stage and returned to unity when the second loading is applied. Tensile strains when the uniaxial bar is nonlinear viscoelastic are also plotted in figure 3.2. As shown, the finite element prediction and analytical solution are identical. Another observation to be noted from the figure is that instantaneous strains resulting from all four cases are identical, but later stage strains from the nonlinear viscoelastic cases are greater than those from the linear viscoelastic cases. This seems reasonable because the nonlinear parameter g_0^a, which contributes to instantaneous response, was set equal to unity, and the other two parameters that affect later stage responses represented nonlinear viscoelastic behavior. This confirms that the UMAT code equipped with the nonlinear viscoelastic feature was developed appropriately and can be used to simulate nonlinear viscoelastic responses of general structures (such as pavements) that are typically associated with complicated geometry and boundary conditions.

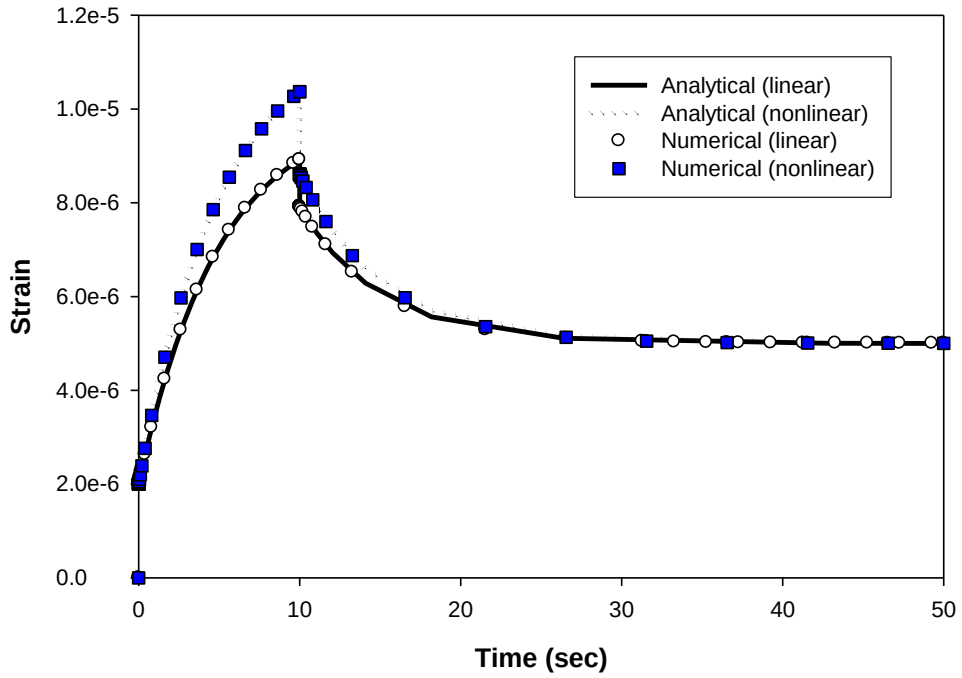

Figure 3.2 Code verification results: Comparisons between analytical and numerical

3.2 Cohesive Zone Model

The FPZ is a nonlinear zone characterized by progressive softening, for which the stress decreases at increasing deformation. The nonlinear softening zone is surrounded by a non-softening nonlinear zone, which represents material inelasticity. Bazant and Planas (1998) classified the fracture process behavior in certain materials into three types: brittle, ductile, and quasi-brittle. Each type presents different relative sizes of these two nonlinear zones (i.e., softening and non-softening nonlinear zones). Figure 3.3 presents the third type of behavior, so-called quasi-brittle fracture. It includes situations in which a major part of the nonlinear zone undergoes progressive damage with material softening due to microcracking, void formation, interface breakages, frictional slips, and others. The softening zone is then surrounded by the inelastic material yielding zone, which is much smaller than the softening zone. This behavior

includes a relatively large FPZ, as illustrated in figure 3.3. Asphaltic paving mixtures are usually classified as quasi-brittle materials (Bazant and Planas 1998; Duan et al. 2006; Kim et al. 2008).

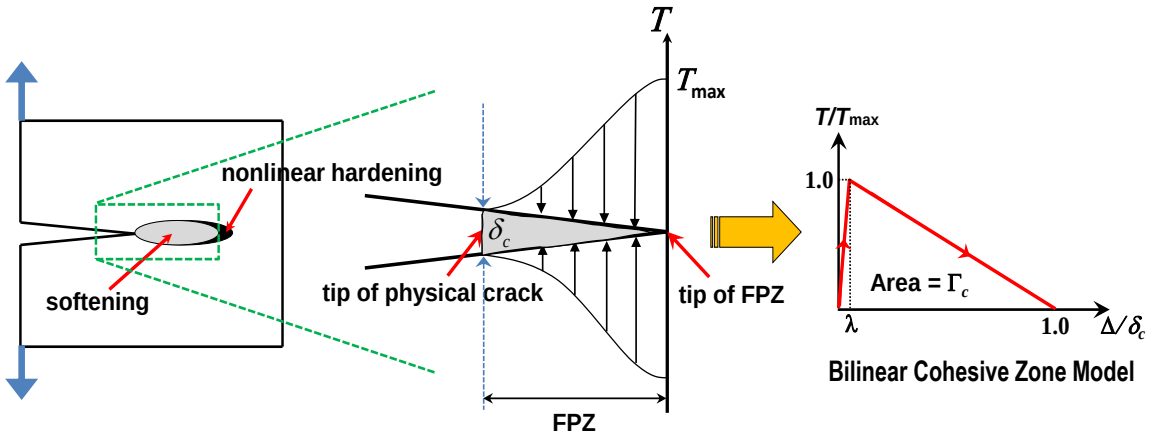

Figure 3.3 Schematic illustration of FPZ of typical quasi-brittle materials

The FPZ can be modeled in many different ways. One well-known approach is to use a cohesive zone. At the crack tip, the cohesive zone constitutive behavior reflects the change in the cohesive zone material properties due to microscopic damage accumulation ahead of the crack tip. This behavior can be expressed by the general traction-displacement cohesive zone relationship as follows:

$$T_i(x_m, t) = T_i\{\Delta_i(x_m, \tau)\} \tag{3.19}$$

where,

T_i = cohesive zone traction (T_n for normal and T_t for tangential traction),

Δ_i = cohesive zone displacement (Δ_n for normal and Δ_t for tangential displacement),

x_m = spatial coordinates, and

t = time of interest.

Cohesive zone models regard fracture as a gradual phenomenon in which separation (Δ) takes place across an extended crack tip (or cohesive zone) and where fracture is resisted by cohesive tractions (T). The cohesive zone effectively describes the material resistance when material elements are being displaced. Equations relating normal and tangential displacement jumps across the cohesive surfaces with the proper tractions define a cohesive zone model. Among numerous cohesive zone models developed for various specific purposes, this study used an intrinsic bilinear cohesive zone model (Geubelle and Baylor 1998; Espinosa and Zavattieri 2003; Song et al. 2006). As shown in figure 3.3, the model assumes that there is a recoverable linear elastic behavior until the traction (T) reaches a peak value, or cohesive strength ($T_{\max}$) at a corresponding separation in the traction-separation curve. At that point, a non-dimensional displacement (λ) can be identified and used to adjust the initial slope in the recoverable linear elastic part of the cohesive law. This capability of the bilinear model to adjust the initial slope is significant, because it can alleviate the artificial compliance inherent to intrinsic cohesive zone models. The λ value was determined through a convergence study designed to find a value sufficiently small enough to guarantee a level of initial stiffness that renders artificial compliance

of the cohesive zone model insignificant. It was observed that a numerical convergence can be met when the effective displacement is smaller than 0.0005, which was used for simulations in this study. Upon damage initiation, T varies from $T_{\max}$ to 0, when a critical displacement (δ_c) is reached and the faces of the cohesive element are fully and irreversibly separated. The cohesive zone fracture energy (Γ_c), which is the locally estimated fracture toughness, can then be calculated by computing the area below the bilinear traction-separation curve with peak traction ($T_{\max}$) and critical displacement (δ_c) as follows:

$$\Gamma_c = \frac{1}{2}\delta_c T_{\max} \tag{3.20}$$

Chapter 4 Materials and Laboratory Tests

This chapter briefly describes the materials used and the laboratory tests performed in this study. An asphalt mixture was selected for creep-recovery tests at varying stress levels in order to determine its linear and nonlinear viscoelastic material characteristics. The SCB fracture test was conducted at the same testing temperature (30^{o}C) to identify fracture properties of the mixture.

4.1 Materials

Table 4.1 summarizes mixture information, including Superpave PG asphalt binder grade, aggregate gradation of the mixture, and resulting binder content to satisfy mixture volumetric requirements. Binder content of 6.00% was determined as an appropriate value that satisfied all key volumetric characteristics of the asphalt mixture including the 4% ± 1% air voids.

Table 4.1 Mixture information

Mixture ID	Binder PG	Aggregate Gradation (% Passing on Each Sieve)									% Binder	% Voids
		19mm	12.5mm	9.5mm	#4	#8	#16	#30	#50	#200		
AC Mixture	64-28	100	95	89	72	36	21	14	10	3.5	6.00	4.09

4.2 Specimen Fabrication

To conduct the uniaxial static creep-recovery tests, a Superpave gyratory compactor was used to generate the cylindrical samples with a diameter of 150 mm and an approximate height of 170 mm. The compacted samples were then cored and sawed to produce testing specimens targeting an air void of 4% ± 0.5% with a diameter of 100 mm and a height of 150 mm. Figure 4.1 presents a specimen after the compaction and coring-sawing process.

Figure 4.1 A specimen cored and sawn from the gyratory compacted sample

To measure the axial displacement of the specimen under the static compressive force, epoxy glue was used to fix mounting studs to the surface of the specimen so that the three linear variable differential transformers (LVDTs) could be attached to the surface of the specimen at 120^{o} radial intervals with a 100 mm gauge length, as illustrated in figure 4.2. Next, the specimen was mounted in the UTM-25kN testing station for creep-recovery testing (fig. 4.3).

Figure 4.4 demonstrates the specimen production process for the SCB fracture test using the Superpave gyratory compactor and saw machines. The Superpave gyratory compactor was used to produce tall compacted samples: 150 mm in diameter and 175 mm in height. Five slices (each with a diameter of 150 mm and a height of 25 mm) were obtained by removing the top and bottom parts of the tall sample. Finally, the slice was cut into two identical halves, and the saw machine was used to make a vertical notch 25 mm long and 2.5 mm wide.

Figure 4.2 A device used to place the mounting studs for LVDTs

Figure 4.3 A specimen with LVDTs mounted in the UTM-25kN

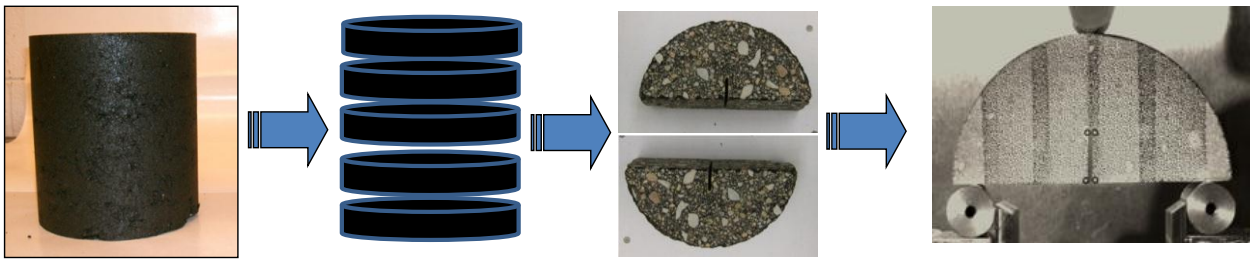

Figure 4.4 SCB specimen fabrication and fracture testing configuration

In this study, the digital image correlation (DIC) system was incorporated with the SCB fracture test to characterize fracture properties of the asphalt mixture. The DIC recognizes the

surface structure of the specimen in digital video images and allocates coordinates to the image pixels. The first image represents the undeformed state, and further images are recorded during the deformation of the specimen. Then, the DIC compares the digital images and calculates the displacement and deformation of the specimen. In order to facilitate the DIC process more efficiently, the specimen was painted with black and white spray until a clear contrast between the white background and numerous black dots (creating an image pattern) was achieved. A number of black dots were used as material points for the full-field deformation characteristics such as formation and movement of the FPZ, as cracks grew due to loading. Additionally, two pairs of dot gauges were attached to the surface of the specimen to more accurately capture the displacements at the mouth (denoted as notch mouth opening displacements [NMOD]) and at the tip (denoted as notch tip opening displacements, [NTOD]) of the initial notch. The DIC system used in this study incorporated a high-speed video camera that can accurately monitor specimen deformation in strains from 0.05% up to 500%. Figure 4.5 shows the SCB testing set-up, painted black dot image pattern, and the additional two-pair gauge points attached on the specimen surface for DIC analysis.

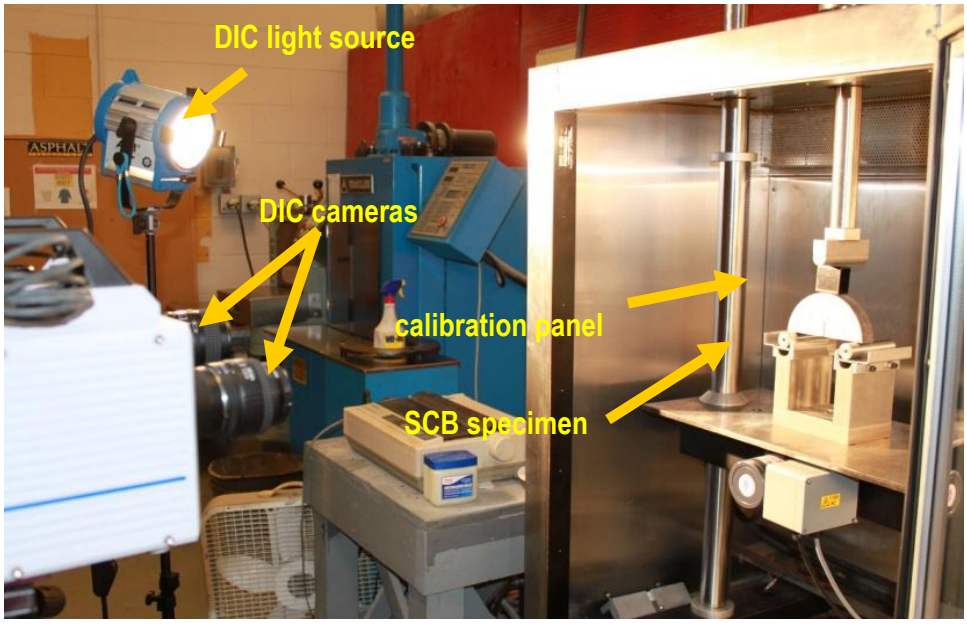

(a) an overview of the whole testing set-up

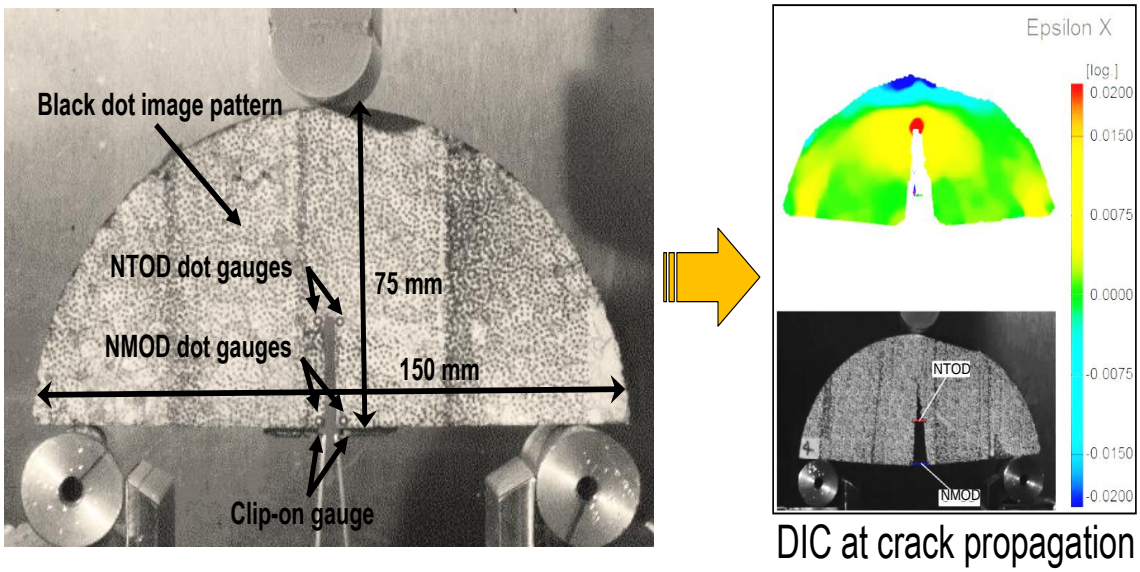

(b) a closer view of a SCB specimen ready to be tested

Figure 4.5 An overview and a closer view of SCB fracture testing

4.3 Creep-Recovery Test

The static creep-recovery test was conducted on replicate specimens of the asphalt mixture at 30^{o}C. A creep stress for 30 seconds (followed by recovery for 1,000 seconds) was applied to the specimens, and the vertical deformation (in compression) was monitored with the three LVDTs. Various stress levels were applied to characterize nonlinear behavior of asphalt mixtures for a large range of stress levels.

Table 4.2 presents applied stress levels and the testing temperature. Based on the preliminary test results, the threshold stress (reference stress) of nonlinear viscoelasticity was found to be 700 kPa. In other words, the asphalt mixture is considered linear viscoelastic below the reference stress level at that testing temperature. Figure 4.6 presents the test results. As expected, the higher stress level generated larger creep strain and recovered less strain.

Table 4.2 Applied stress levels for each mixture

Mixture ID	Temp.	Stress Level (kPa)				
AC Mixture	30°C	700	1,000	1,200	1,500	

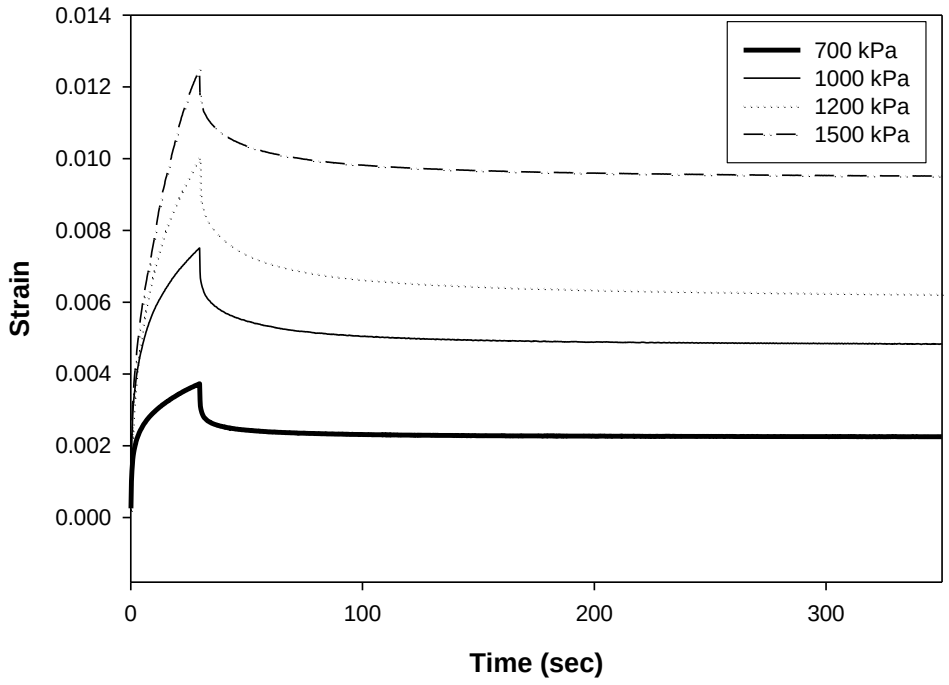

Figure 4.6 Creep-recovery test results at various stress levels

4.4 SCB Fracture Test

A total of 12 SCB specimens of the asphalt mixture were prepared to complete three replicates per test case. Prior to testing, individual SCB specimens were placed inside the environmental chamber of a mechanical testing machine for temperature equilibrium targeting the testing temperature of 30˚C. Following the temperature conditioning step, specimens were subjected to a simple three-point bending configuration with four different monotonic displacement rates (i.e., 1, 5, 10, and 50 mm/min.) applied to the top center line of the SCB specimens. As shown in figure 4.5, metallic rollers separated by a distance of 122 mm (14 mm from the edges of the specimen) were used to support the specimen. Reaction force at the loading point was monitored by the data acquisition system installed in the mechanical testing machine.

Figure 4.7 presents the SCB test results by plotting the average values between the reaction forces and opening displacements (NMOD and NTOD) monitored by the DIC system at

different loading rates. The test results among the replicates at the same testing conditions were repeatable without large discrepancies. The coefficient of variation in the peak force from each testing case was between 5.4% and 10.8%. As clearly illustrated in the figure, the peak force increased as the loading rate increased. The figures confirm that the fracture behavior at the testing temperature of 30˚C was rate-dependent.

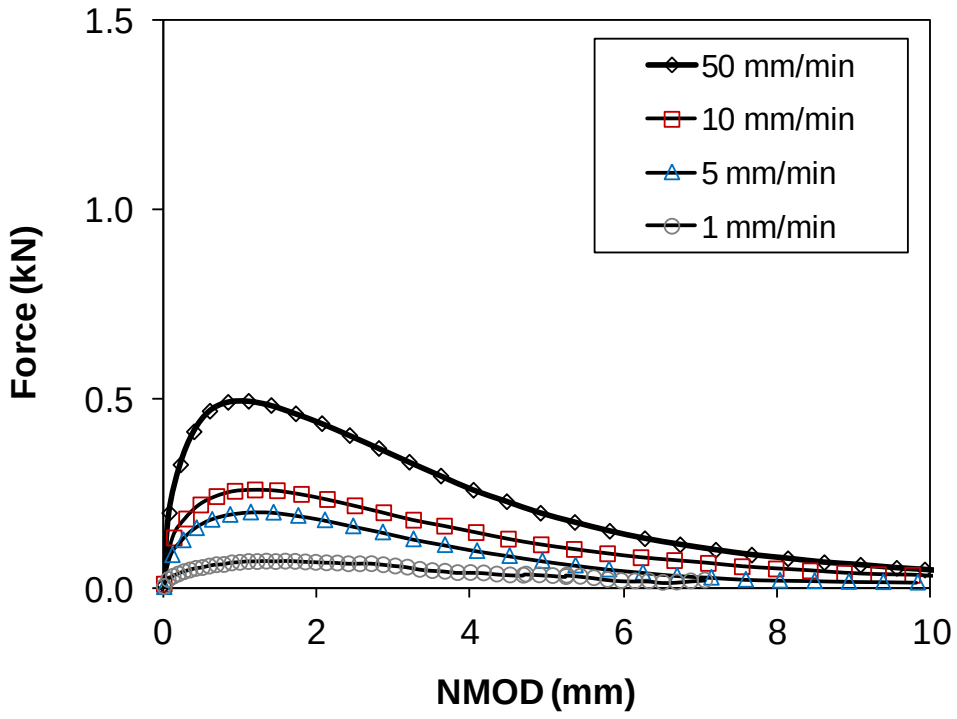

(a) Force-NMOD curves

Figure 4.7 SCB test results at different loading rates and at 30˚C

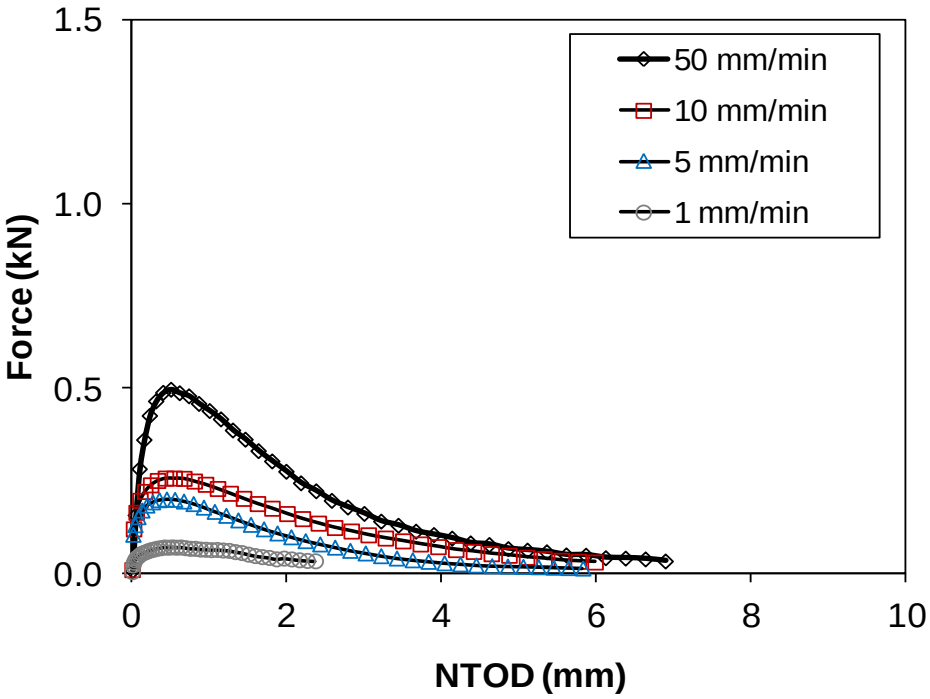

(b) Force-NTOD curves

Figure 4.7 SCB test results at different loading rates and at 30˚C (cont'd.)

Chapter 5 Characterization of Material Properties

In this chapter, the creep-recovery test and SCB fracture test results presented in the previous chapter are used to characterize material properties. Using creep-recovery test results, the linear viscoelastic properties at the threshold stress level are identified, as are the nonlinear viscoelastic properties at higher stress levels. The viscoelastic material properties are then validated by comparing test results with numerical simulations of the creep-recovery test. Regarding the SCB fracture, test results are used to determine fracture properties of the mixture. The cohesive zone fracture properties in the bilinear cohesive zone model are determined for each case through the calibration process until a good agreement between test results and finite element simulations is observed.

5.1 Viscoelastic Material Properties

A schematic of a single creep-recovery test is illustrated in figure 5.1 for a constant stress loading and unloading condition. For loading time period (i.e., $0 < t < t_1$) and unloading period ($t > t_1$), Equation 5.1 can be expressed, respectively, in terms of creep strain (ε_c) and recovery strain (ε_r) as:

$$\varepsilon_c(t) = g_0 D_0 \sigma + g_1 g_2 \sigma \Delta D\left(\frac{t}{a_\sigma}\right) \tag{5.1}$$

$$\varepsilon_r(t) = g_2 \sigma \left[\Delta D\left(\frac{t_1}{a_\sigma} + t - t_1\right) - \Delta D(t - t_1)\right] \tag{5.2}$$

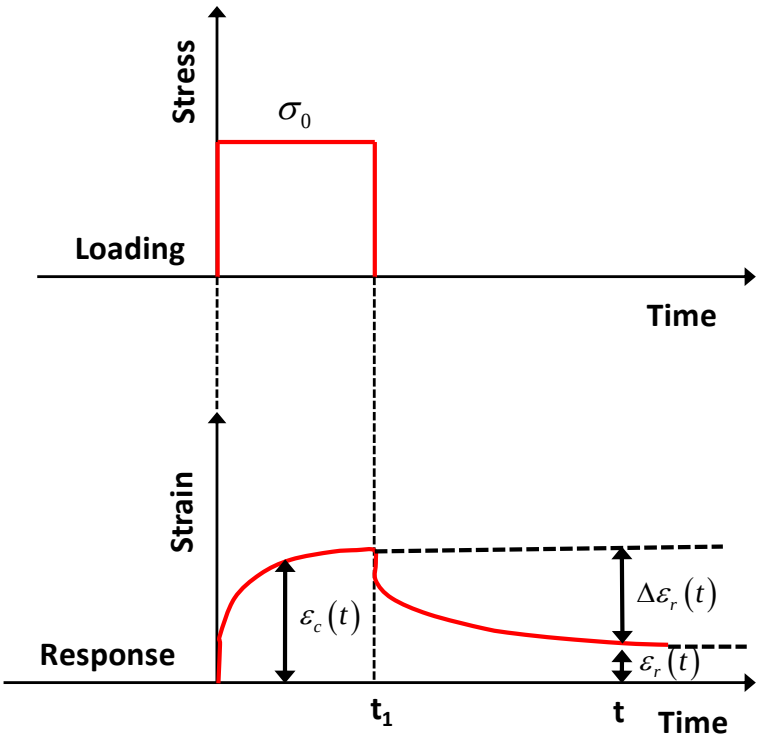

Figure 5.1 A schematic of a single creep-recovery test

The first step was to obtain the Prony series coefficients in equation 3.3 from linear viscoelastic response at the threshold stress level of each considered temperature. Since the recoverable response is linear viscoelastic ($g_0 = g_1 = g_2 = a_\sigma = 1$) at the threshold stress level, the recovered strain $\Delta\varepsilon_r(t)$ shown in figure 5.1 can be used to obtain the linear viscoelastic Prony series coefficients. Substituting equation 3.3 into equations 5.1 and 5.2 yields:

$$\begin{aligned}\Delta\varepsilon_r(t) &= \varepsilon_c(t_1) - \varepsilon_r(t) \\ &= \sigma\left\{\begin{array}{l}\sum_{n=1}^{N} D_n\left[1-\exp\left(-\lambda_n t_1\right)\right]- \\ \sum_{n=1}^{N} D_n\left[1-\exp\left(-\lambda_n t\right)\right]+\sum_{n=1}^{N} D_n\left[1-\exp\left(-\lambda_n\left(t-t_1\right)\right)\right]\end{array}\right.\end{aligned} \tag{5.3}$$

Next, Prony series coefficients were determined by minimizing error between experimental measurements and predicted strains using equation 5.3. Resulting coefficients of each mixture are listed in table 5.1.

Table 5.1 Viscoelastic properties determined through the characterization process

N	λ_n (s^{-1})	D_n (MPa^{-1}) of Mixture 1 at 30°C
1	10^2	6.70×10^{-4}
2	10	8.91×10^{-5}
3	1	5.17×10^{-4}
4	10^{-1}	6.45×10^{-4}
5	10^{-2}	9.47×10^{-4}
6	10^{-3}	2.60×10^{-4}
7	10^{-4}	2.73×10^{-4}
8	10^{-5}	7.54×10^{-4}

Once the linear viscoelastic Prony series coefficients were obtained, the nonlinear viscoelastic parameters at higher stress levels could be determined. The recovered strains at high stress levels were again used, under the assumption that the transient creep compliance is expressed in the form of a power law as follows:

$$\Delta D(\psi) = D_c \psi^n \tag{5.4}$$

where,

D_c and n are material constants.

Substituting equation 5.4 into equations 5.1 and 5.2 gives:

$$\begin{aligned}\Delta\varepsilon_r(t) &= \varepsilon_c(t_1) - \varepsilon_r(t) \\ &= \alpha^* - \beta^*\left[(1+a_\sigma\eta)^n - (a_\sigma\eta)^n\right]\end{aligned} \tag{5.5}$$

where,

$$\alpha^* = g_0 D_0 \sigma + g_1 g_2 D_c \sigma \left(\frac{t_1}{a_\sigma}\right)^n \tag{5.6}$$

$$\beta^* = g_2 D_c \left(\frac{t_1}{a_\sigma}\right)^n \tag{5.7}$$

$$\eta = \frac{t - t_1}{t_1} \tag{5.8}$$

Fitting equation 5.5 to the recovered strains $\Delta\varepsilon_r$ can determine constants: n, α^*, β^*, and a_σ. It is noted that n is nearly stress-independent, and can be obtained at a low stress level (Lai and Bakker, 1996); therefore, the n value was fixed as a constant, and the values of α^*, β^* and a_σ were obtained by repeating the fitting process. Next, g_2 was determined by minimizing errors between experimental data and equation 5.7. Similarly, g_0 and g_1 were determined from equation 5.6. Table 5.2 presents the stress-dependent nonlinear viscoelastic parameters of the asphalt mixture tested at 30°C. Nonlinear viscoelastic parameters in table 5.2 indicate that g_1 was not significantly related to nonlinearity, whereas other parameters such as g_0 and g_2 were sensitive to stress levels. Both parameters generally increased as higher stresses were involved.

Table 5.2 Nonlinear viscoelastic parameters determined

Parameters	AC Mixture at 30°C		
	Polynomial constants, *i*		
	1	2	3
g_0 (α_i)	0.05	0.77	-0.54
g_1 (β_i)	0	0.01	-0.01
g_2 (γ_i)	0.36	0.83	-0.71
a_σ (δ_i)	-0.14	0.84	-0.83

After obtaining the viscoelastic material properties (both linear and nonlinear), model validation was conducted by comparing finite element model simulations to the creep-recovery test results. For simplicity, one element of a single creep-recovery test was simulated using the obtained material properties (i.e., Prony series coefficients and nonlinear viscoelastic parameters presented in table 5.1 and table 5.2).

Figure 5.2 presents the comparisons of recovered strains between experimental results and numerical predictions. As shown in the figure, for the cases at threshold stress levels (700 kPa), results between testing and simulation are almost identical. As the level of stress becomes higher, slight discrepancies between testing and simulation are observed; however, overall simulation results show good agreement with the experimental data. This indicates that the developed UMAT is working properly and can be used to simulate the linear-nonlinear viscoelastic response of multilayered pavement structures, which is described in a later section.

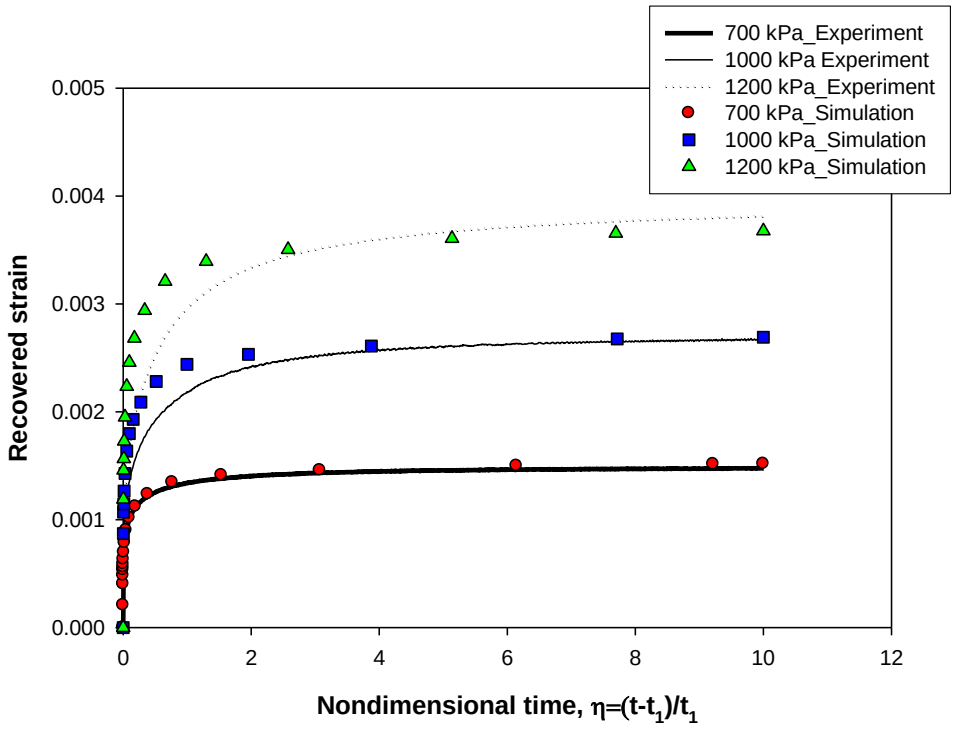

Figure 5.2 Comparison plots between model predictions and test results

The proposed approach, based on the nonlinear viscoelastic characteristics, is expected to provide much better identification of mechanical behavior in comparison to simple linear viscoelastic modeling, where mixtures are subject to higher service temperatures and heavy vehicle loads. However, in those conditions, a considerable amount of plastic (irrecoverable) strains are usually involved, which implies that a more accurate constitutive model would require plastic and/or viscoplastic contribution in conjunction with the nonlinear viscoelastic characteristics, in order to comprehensively account for overall mechanical behavior. Several studies have pursued constitutive modeling with plastic or viscoplastic components. Zhao (2002) incorporated viscoelastic-plastic behavior with growing damage based on Schapery's continuum damage theory and Uzan's strain hardening model. Yoo (2007) performed three-dimensional finite element analysis to calculate creep strains due to heavy vehicular loading cycles, using

nonlinear time-hardening creep models to characterize the creep behavior of asphalt mixtures at intermediate and high temperatures. More recently, Huang et al. (2011) developed a nonlinear viscoelastic-viscoplastic constitutive model and implemented it into a 3-D finite element model. The study showed that finite element simulations can capture pavement responses under repeated loading at different temperatures. Although the plastic component is considered necessary to more appropriately account for overall mechanical behavior, it was not taken into consideration for the current study.

5.2 Fracture Properties

Fracture properties of the asphalt mixture were determined by numerical simulations of the SCB fracture tests. This was implemented to identify fracture characteristics along the FPZ, which is locally associated with initiation and propagation of cracks through the SCB specimens. As noted earlier, finite element model simulations incorporated with the cohesive zone fracture can be effectively applied to examine the local fracture behavior, since the cohesive zone effectively describes the material resistance to fracture when material elements in a real length scale are being displaced.

Figure 5.3 presents a finite element mesh, which was finally selected after conducting a mesh convergence study. The specimen was discretized using two-dimensional, three-node triangular linear prism elements for the bulk specimen. Four-node, zero-thickness cohesive zone elements were inserted along the center of the mesh to permit mode I crack growth in the simulation of SCB testing. The bilinear cohesive zone model illustrated in figure 3.3 was used to simulate fracture in the middle of the SCB specimen as the opening displacements increased. It should be noted that the simulation conducted herein involves several limitations at this stage as a result of assuming the mixture to be homogeneous and isotropic with only mode I crack

growth—which may not represent the true fracture process of specimens specifically tested at the ambient temperatures where mixture heterogeneity (i.e., microstructural characteristics) and mixed-mode fracture is not trivial (fig. 5.3).

The cohesive zone fracture properties (two independent values of the three: T_{max}, δ_c, and Γ_c) in the bilinear model were determined for each case through the calibration process until a good match between test results and numerical simulations was observed. Figures 5.4 and 5.5 present good agreements between the test results (average of the three SCB specimens per case) and finite element simulations. Resulting fracture properties (T_{max} and Γ_c) at each loading rate are presented in table 5.3. The good agreement between tests and model simulations indicates that the local fracture properties were properly defined through the integrated experimental-numerical approach.

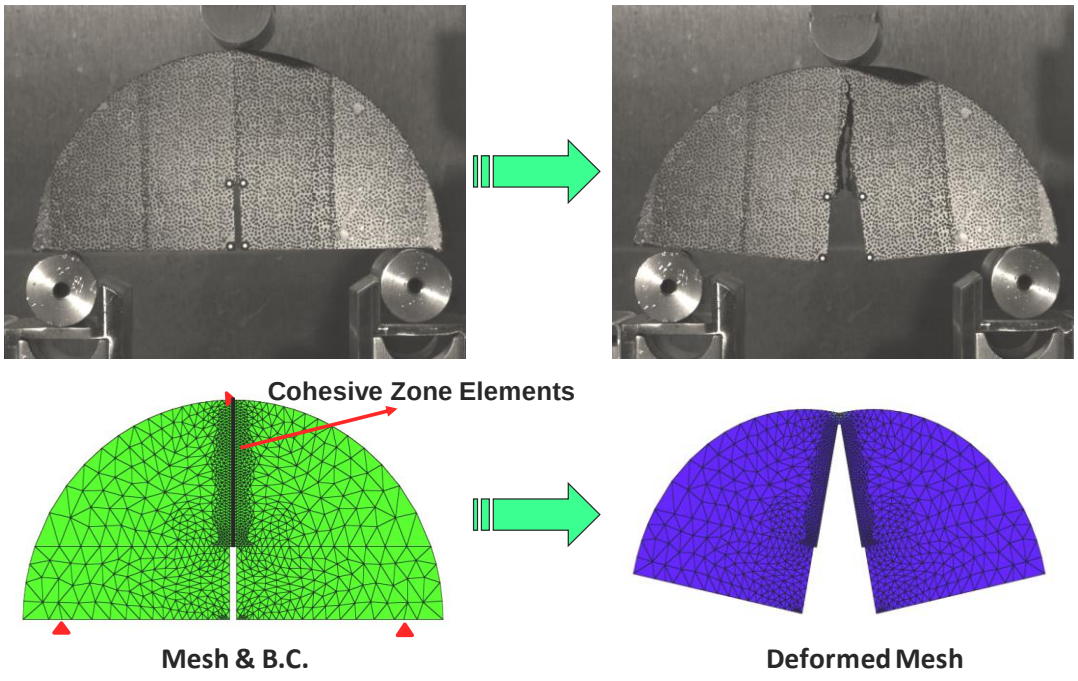

Figure 5.3 A finite element modeling of the SCB testing

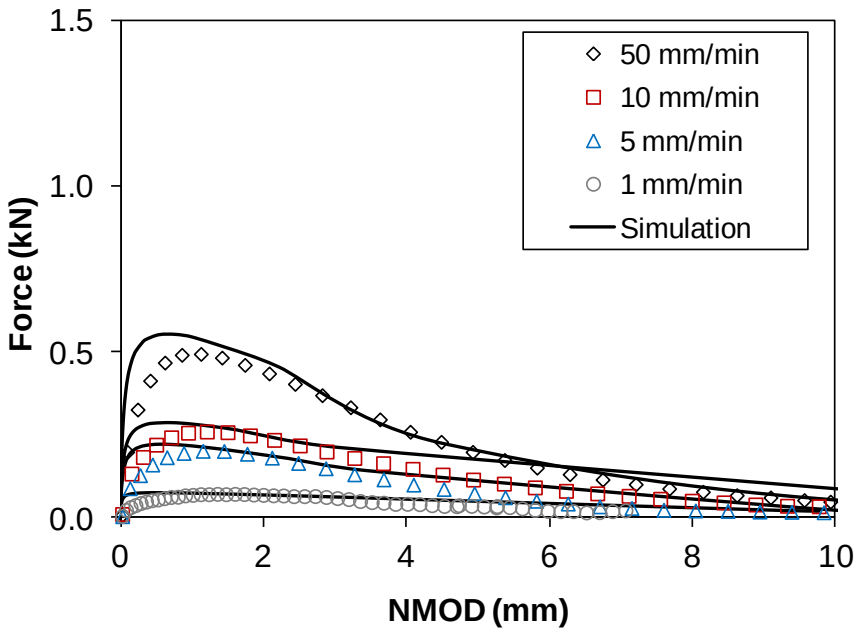

Figure 5.4 SCB test results vs. cohesive zone model simulation results (force-NMOD)

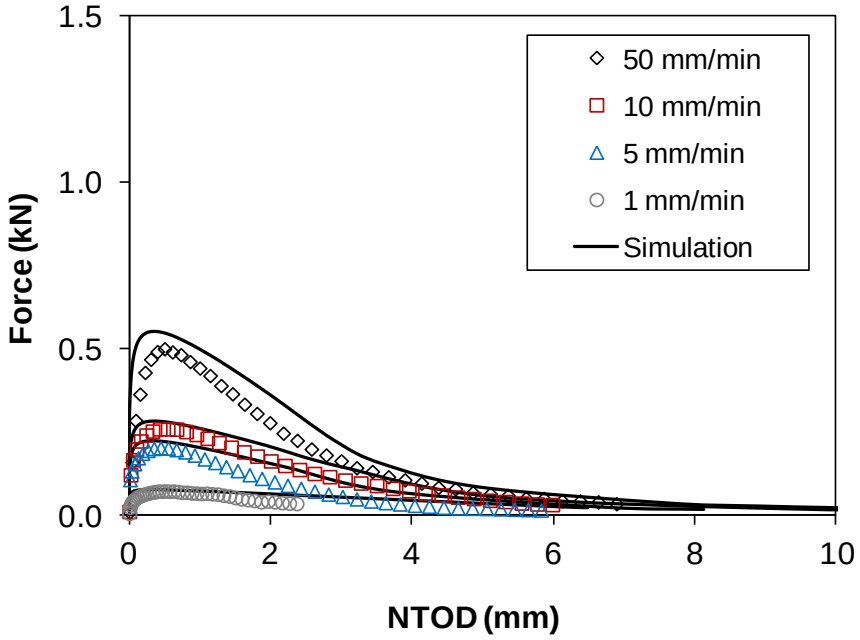

Figure 5.5 SCB Test results vs. cohesive zone model simulation results (force-NTOD)

Table 5.3 Cohesive zone fracture parameters determined

Temperature (^{o}C)	Loading Rate (mm/min.)	Cohesive Zone Fracture Parameters	
		T_{max} (kPa)	Γ_c (J/m^2)
30	1	8.0E+01	220
	5	2.5E+02	400
	10	3.2E+02	550
	50	6.5E+02	900

The values presented in table 5.3 clearly suggest that the consideration of material viscoelastic constitution for the bulk body is not itself adequate to predict the fracture behavior of asphalt mixtures. Other sources of rate-dependence, such as the local rate-dependent fracture behavior at the fracture process zone, are also necessary for more accurate analyses and designs.

Chapter 6 Finite Element Analysis of Pavement

In this chapter, a typical pavement structure used in Nebraska was modeled through the 2-D finite element method, in order to investigate the mechanical performance behavior of the pavement when subjected to heavy truck loading. The 2-D finite element modeling was conducted using a commercial package, ABAQUS Version 6.8 (2008), which was incorporated with the cohesive zone fracture and the developed nonlinear viscoelastic UMAT. Simulation results comparing responses from linear viscoelasticity and from the use of nonlinear viscoelastic material characteristics with and without the cohesive zone fracture are presented and discussed in this chapter.

6.1 Pavement Geometry and Boundary Conditions

A typical pavement structure used in Nebraska was selected for simulations. Figure 6.1 illustrates a four-layered asphalt pavement structure (101.6 mm thick asphalt layer, 254 mm Portland cement concrete (PCC) layer with PCC joints, 101.6 mm bituminous foundation course (BFC) and 152.4 mm subgrade). Both sides of the vertical edge of the finite element pavement model were fixed in the horizontal direction, and the bottom of the model was fixed in the vertical direction to represent a rock foundation. To reduce computational time, graded meshes, which have finer elements close to the potential separation/distress regions, were used (fig. 6.1). The red line in the figure indicates the region where cohesive zone elements were inserted in the mesh to allow cracking (reflective and/or top-down). A tire pressure of 720 kPa and axial load of 35.5 kN were applied to the pavement based on a study by Yoo (2007).

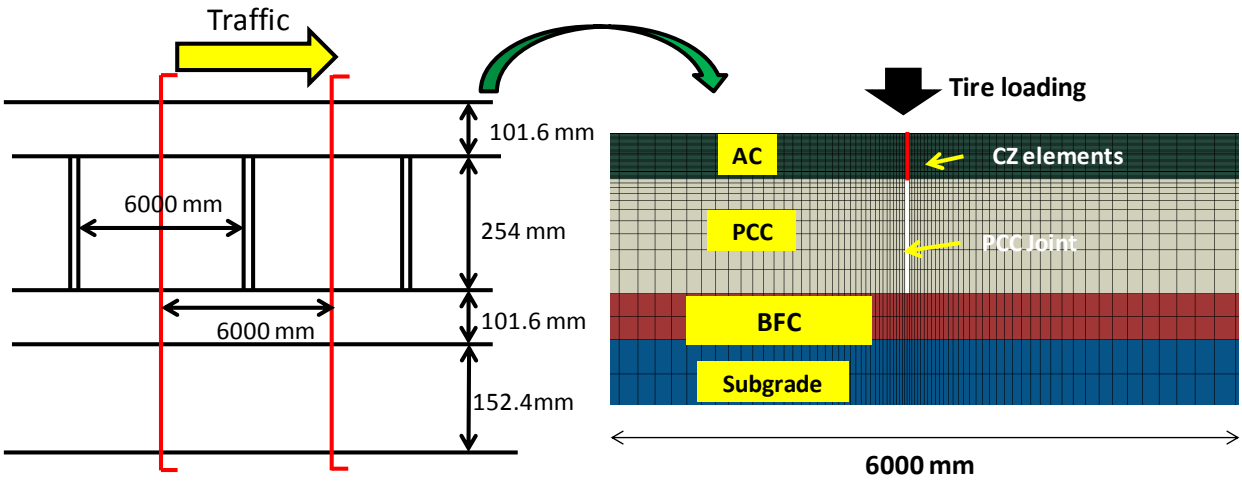

Figure 6.1 A pavement geometry and boundary conditions for finite element modeling

Figure 6.2 illustrates the loading configuration of the Class 9 truck used in this study (Soares et al. 2008). Although the truck loading consisted of a front steer axle and two tandem axles with dual tires, in order to reduce computational time in the analysis, only the two tandem axles with dual tires were applied through use of the trapezoidal loading sequence shown in the figure. A 15.4 m Class 9 truck trailer traveling at 80 km/h takes 0.692 seconds to pass over a fixed point on the pavement. Therefore, the first truck passes the fixed point for 0.692 seconds and, after 30 seconds, a second truck passes through the same point. The passage of a total of 50 trucks was simulated.

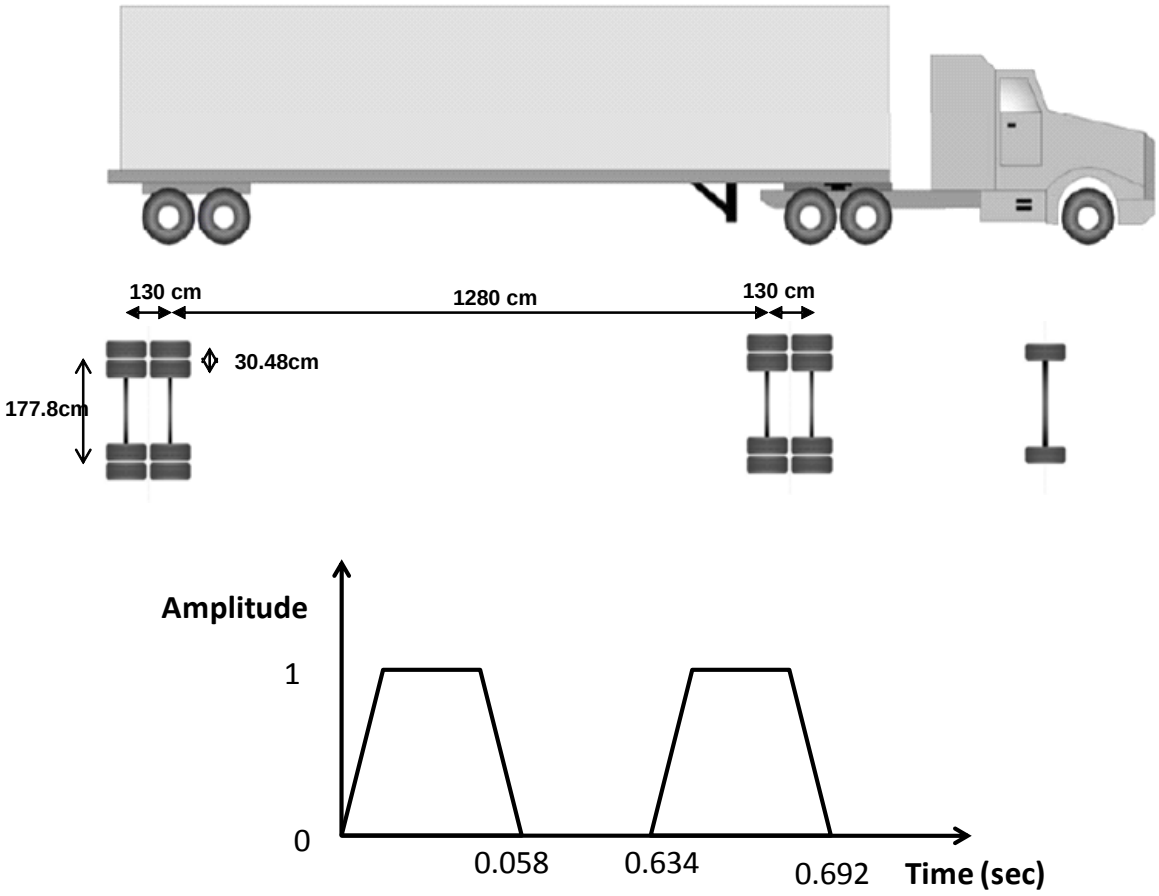

Figure 6.2 Truck loading configuration (Class 9) used in this study

6.2 Layer Properties

Table 6.1 presents material properties of the individual layers. The underlying layers (i.e., PCC, BFC, and subgrade) were modeled as isotropic linear elastic, while viscoelastic response was considered to describe the behavior of the asphalt concrete surface layer. The surface layer can dissipate energy due to its viscoelastic nature and cohesive zone, which results in permanent deformation (rutting) and fracture of the layer. Different performance responses between the linear and nonlinear viscoelastic approaches with and without cohesive zone fracture were

compared, and the resulting significance of the nonlinear viscoelastic nature and the cracking of asphalt mixtures was observed.

Table 6.1 Material properties of each layer

Linear Elastic Material Properties				
Layer	E (MPa)			υ
PCC	152			0.3
BFC	26,200			
Subgrade	43			
Cohesive Zone Fracture Properties of Asphalt Surface				
Γ_c (J/ m^2)	400			
T_{max} (kPa)	250			
Linear Viscoelastic Properties of Asphalt Concrete Surface				
	n	λ_n (s^{-1})	D_n (MPa^{-1})	
Asphalt Concrete	1	10^2	6.70x10^{-4}	
	2	10	8.91x10^{-5}	
	3	1	5.17x10^{-4}	
	4	10^{-1}	6.45x10^{-4}	
	5	10^{-2}	9.47x10^{-4}	
	6	10^{-3}	2.60x10^{-4}	
	7	10^{-4}	2.73x10^{-4}	
	8	10^{-5}	7.54x10^{-4}	
Nonlinear Viscoelastic Parameters of Asphalt Concrete Surface				
Asphalt Concrete	Polynomial constants, i			
	Parameters	1	2	3
	$g_0(\alpha_i)$	0.05	0.77	-0.54
	$g_1(\beta_i)$	0	0.01	-0.01
	$g_2(\gamma_i)$	0.36	0.83	-0.71
	$a_\sigma(\delta_i)$	-0.14	0.84	-0.83

6.3 Simulation Results

This subsection presents simulation results and differences in pavement responses among the four attempts, which modeled the asphalt concrete layer using linear viscoelastic properties with or without the cohesive zone fracture and nonlinear viscoelastic properties with or without

the cohesive zone fracture behavior. Among many mechanical responses, the vertical displacement from the pavement surface, the crack opening (horizontal) displacement through the depth of the asphalt concrete layer, and the horizontal strain at the bottom of the asphalt layer were examined with the 50 cycles of truck loading; they are strongly related to the two primary distresses of asphaltic pavement: rutting and cracking.

6.3.1 Permanent Deformation (Rut Depth)

Figure 6.3 compares permanent deformation (rut depth) accumulated from each truck loading up to the 50 cycles. It clearly shows the increasing difference in the rut depth among the four cases as the number of loading cycles increases. At the end of the 50 cycle simulation, the total rut depth predicted from the nonlinear viscoelastic with the cohesive zone fracture was the greatest, while the rut depth simulated from the linear viscoelastic without cohesive zone was the smallest. The figure clearly demonstrates the effects of material characteristics on the overall pavement performance.

Figure 6.4 shows contour plots of vertical displacement distributions in the asphalt layer for different numbers of loading cycles (i.e., 10, 30, and 50 cycles) obtained from the four modeling approaches. Contour plots in the top left-hand-side are results from the simulation of linear viscoelastic without cohesive zone fracture, while the top right-hand-side plots were obtained in consideration of the cohesive zone fracture in the linear viscoelastic asphalt layer. Similarly, contour plots in the bottom left-hand-side were from the simulation of nonlinear viscoelastic without cohesive zone fracture, and the bottom right-hand-side plots present vertical displacement contours resulting from model simulation with nonlinear viscoelasticity and cohesive zone fracture of asphalt layer. These plots clearly show that vertical displacement from the nonlinear viscoelastic model propagates much more quickly to the bottom of the asphalt layer

than does vertical displacement from the linear viscoelastic model when the number of loading cycles is increased. In addition, both linear and nonlinear viscoelastic case with the cohesive zone fracture showed greater vertical displacements at the same loading stage than did those from simulations without the cohesive zone fracture. This clearly indicates that performance-based design of pavement structures should be based on proper characterization of materials.

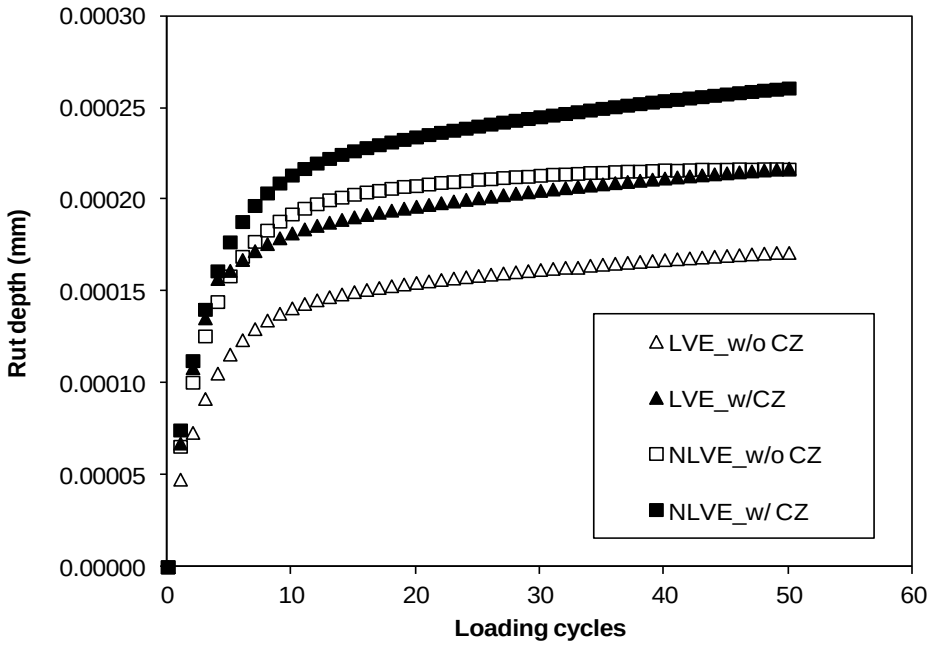

Figure 6.3 Comparison of permanent deformation up to 50 loading cycles

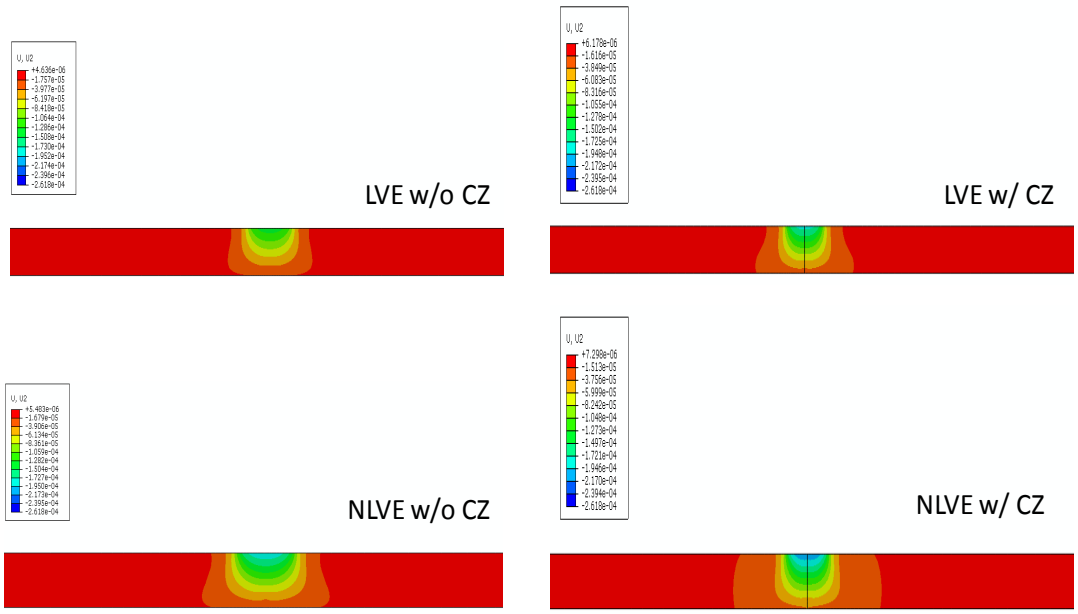

(a) at 10th cycle

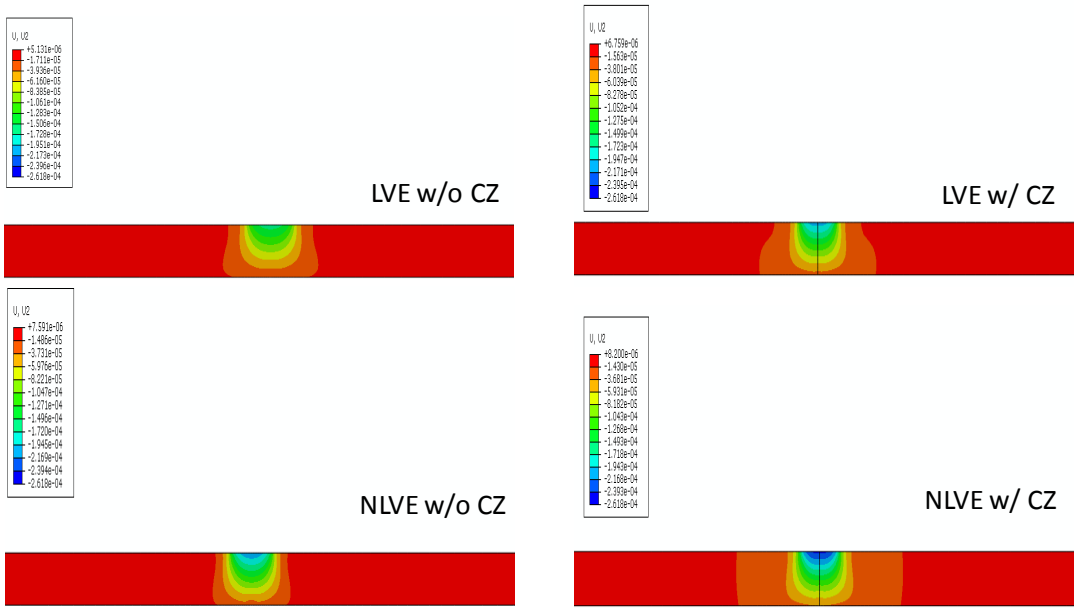

(b) at 30th cycle

Figure 6.4 Contour plots of vertical displacement distributions

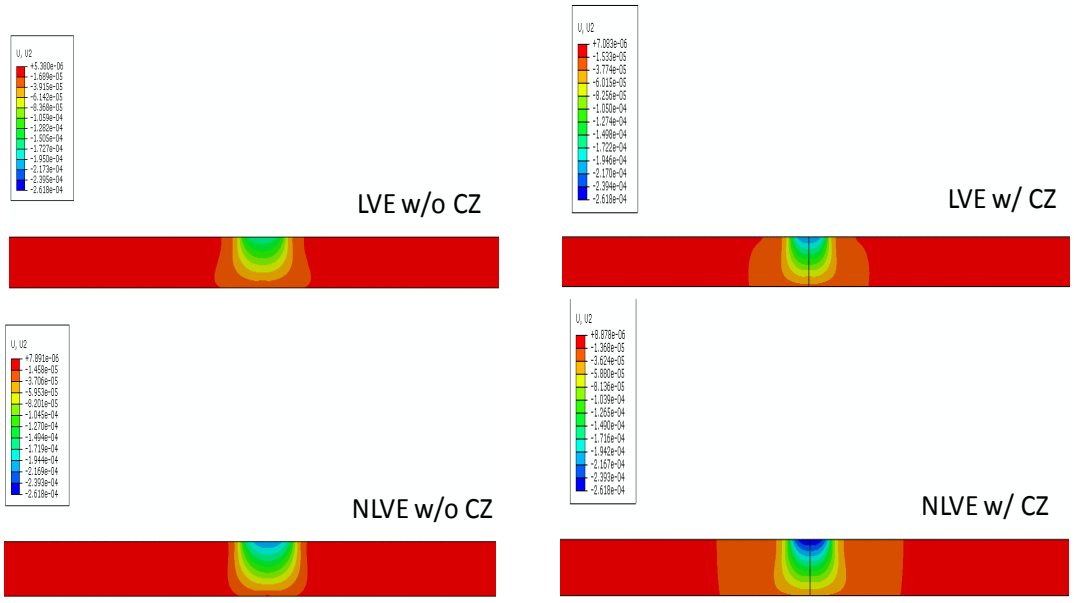

(c) at 50th cycle

Figure 6.4 Contour plots of vertical displacement distributions (cont'd.)

6.3.2 Horizontal Strain

Figure 6.5 shows horizontal strain profiles at the bottom of the asphalt layer for up to 50 truck loading cycles. Note that the sign convention adopted herein is positive for tension. As shown in the figure, the maximum tensile strains take place below the tire, and compressive strains develop between the tires. The nonlinear viscoelastic model predicted greater maximum tensile strains than did the case of linear viscoelastic layer. Regarding the effect of cohesive zone fracture on the horizontal strain at the bottom of the asphalt layer, smaller horizontal strains were monitored from the cases without cohesive zone fracture behavior than from cases with cohesive zones for both linear viscoelastic and nonlinear viscoelastic models.

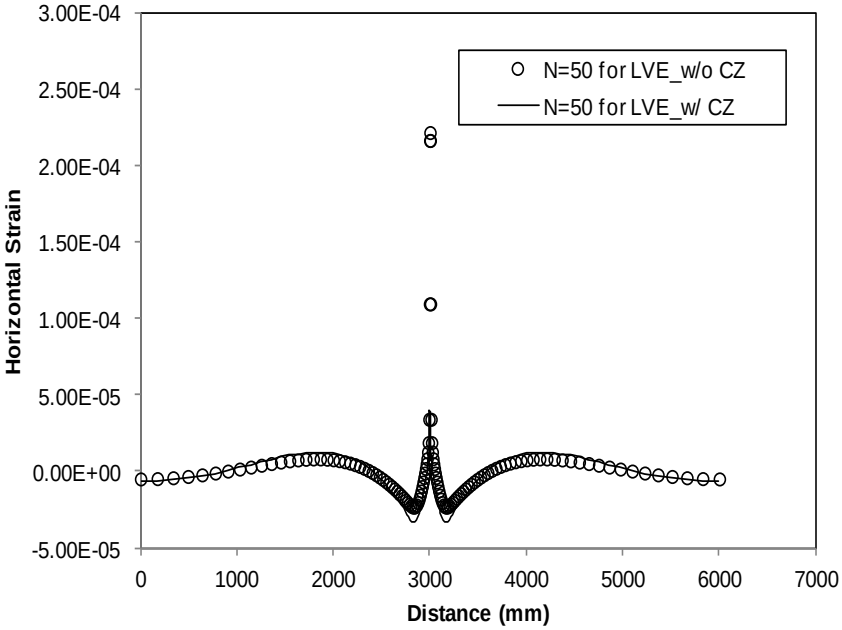

(a) linear viscoelasticity simulations

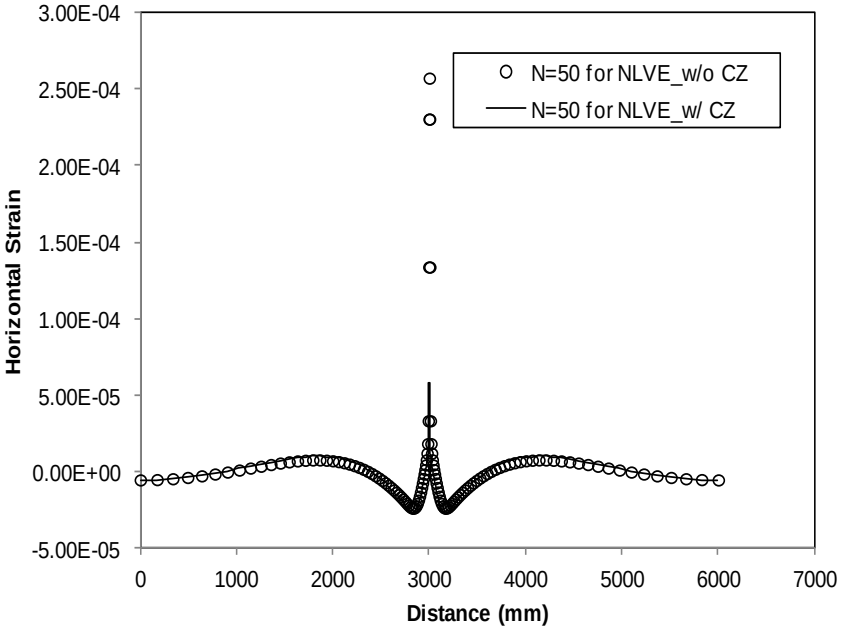

(b) nonlinear viscoelasticity simulations

Figure 6.5 Comparison of horizontal strain plots

6.3.3 Crack Opening

Figure 6.6 shows that tensile stresses occurred through the depth of the asphalt surface layer at the end of 50th loading cycle from the two modeling approaches: linear and nonlinear viscoelastic with the cohesive zone fracture. As illustrated in the figure, the tensile stresses between the two modeling approaches from the top surface to the bottom of 90 mm were the same. However, the nonlinear viscoelastic case with cohesive zone fracture experienced tensile stresses approximately four times greater than those from the linear viscoelastic case at the bottom of the asphalt layer. Consequently, as can be seen in figure 6.7, crack opening displacements between the two cases from the top surface to the bottom of 90 mm were close each other, whereas the two modeling cases presented significant differences in the fracturing of the asphalt at the bottom of the layer.

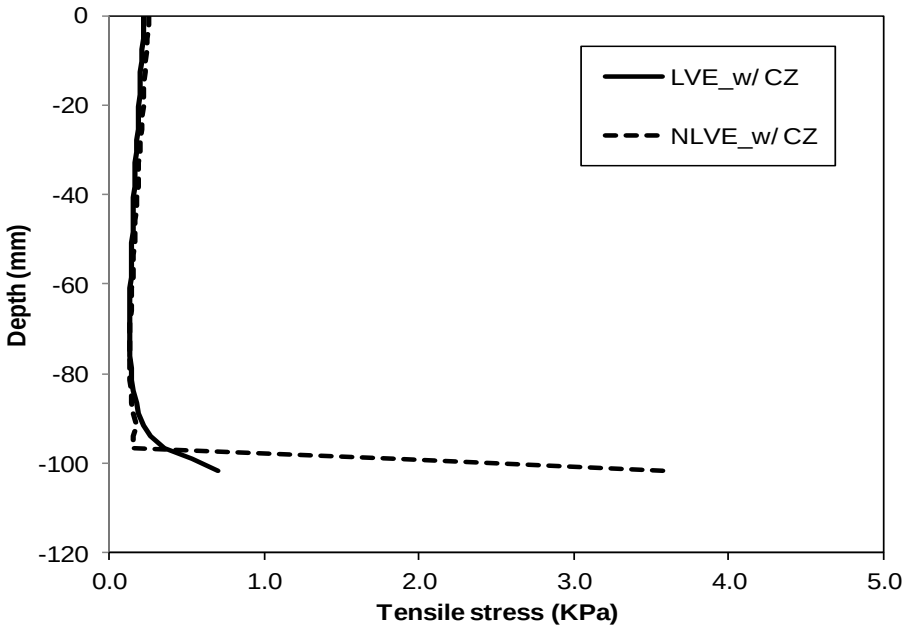

Figure 6.6 Depth-tensile stress curve: LVE vs. NLVE

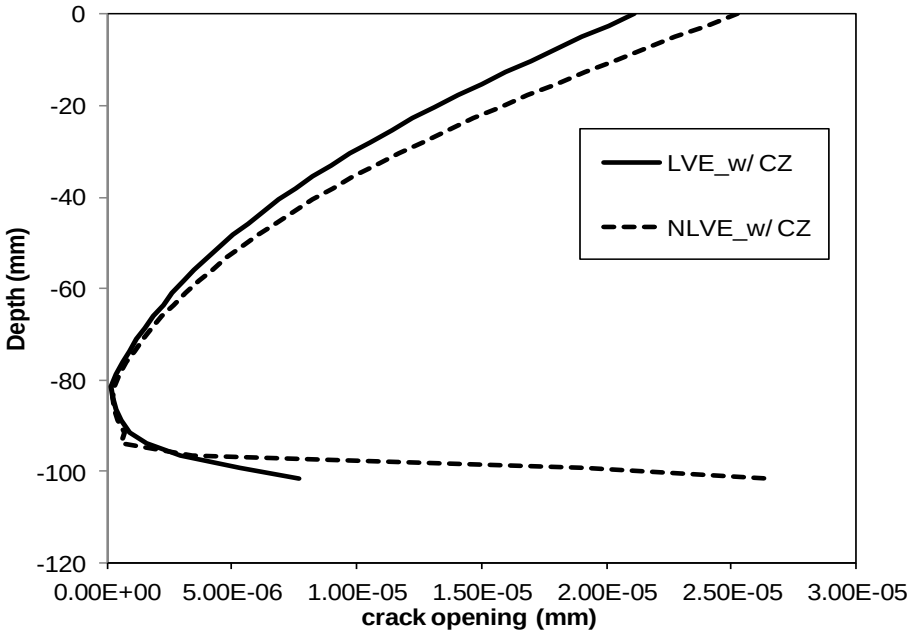

Figure 6.7 Depth-crack opening curve: LVE vs. NLVE

Chapter 7 Summary and Conclusions

As an extension of Ban et al. (2011), we have sought a more advanced constitutive model for asphalt mixtures, in order to more accurately predict pavement responses. To this end, Schapery's nonlinear viscoelastic constitutive model was implemented into the commercial finite element software ABAQUS via a user defined subroutine (UMAT), and the cohesive zone fracture model was involved in the process to more realistically analyze distresses in asphaltic pavements subjected to heavy truck loads. Several laboratory tests (i.e., creep-recovery tests at various stress levels to obtain stress-dependent viscoelastic material properties; semi-circular bending (SCB) fracture tests at different loading rates to identify viscoelastic fracture properties) of an asphalt mixture were conducted. Test results were used to obtain fundamental material properties, which were in turn used to model structural performance of a typical Nebraska asphaltic pavement.

Detailed investigations of the pavement responses resulting from different constitutive relations (i.e., linear viscoelastic and nonlinear viscoelastic with and without cohesive zone fracture) provided interesting observations and findings that could be used to better understand the effects of truck loading on pavement damage, and consequently to further advance current pavement-analysis design methods. The following bullet points summarize the conclusions that can be drawn:

- Schapery's nonlinear viscoelastic model was well implemented into the ABAQUS via a user material subroutine UMAT. An example problem presented in this study verified the model and its numerical implementation.

- Creep-recovery tests at varying stress levels were conducted to identify viscoelastic mixture characteristics. As expected, test results clearly demonstrated stress-dependent mixture characteristics.
- Utilizing the creep-recovery test results, a series of processes was applied to identify linear and nonlinear viscoelastic properties. Linear viscoelastic properties were characterized by the Prony series based on the generalized Maxwell model, and nonlinear viscoelastic parameters were successfully fitted to polynomial functions, which enables the representation of individual nonlinear viscoelastic properties as a continuous function of stress levels.
- At intermediate service temperatures such as 30^{o}C, the rate-dependent fracture behavior was obvious. Cohesive zone fracture properties varied as the loading rate changed.
- Two-dimensional finite element simulations of a pavement structure showed significant differences among the cases (linear viscoelastic vs. nonlinear viscoelastic with and without fracture damage) in the prediction of pavement performance (both rutting and cracking).
- Although test results and numerical simulations presented in this study are limited in their ability to make definitive conclusions, performance differences observed between individual cases are considered significant and should be addressed in the process of performance-based pavement design. These findings imply the necessity of deliberate, accurate, and more realistic characterizations of paving materials.

References

Airey, G., B. Rahimzadeh, and A. C. Collop. 2004. "Linear rheological behavior of bituminous paving material." *Journal of Materials in Civil Engineering*, *16*: 212–220.

American Association of State Highway and Transportation Officials (AASHTO). 2008. Mechanistic-empirical pavement design guide, Interim edition: A manual of practice. Available from https://bookstore.transportation.org

Al-Qadi, I. L., M .A. Elseifi, and P. J. Yoo. 2004. "In-situ validation of mechanistic pavement finite element modeling." *Proceedings of the 2nd International Conference on Accelerated Pavement Testing*, Minneapolis, MN.

Al-Qadi, I. L., A. Loulizi, I. Janajreh, and T. E. Freeman. 2002. "Pavement response to dual and new wide base Tires at the same tire pressure." *Transportation Research Record*, *1806*: 38-47.

Al-Qadi, I. L., P. J. Yoo, and M .A. Elseifi. 2005. "Characterization of pavement damage due to different tire configurations." *Journal of the Association of Asphalt Paving Technologists, 74* : 921-962.

Aragão, F. T. S. 2011. "Computational microstructure modeling of asphalt mixtures subjected to rate-dependent fracture." Ph.D. Diss., University of Nebraska, Lincoln.

Aragão, F. T. S. and Y. Kim. 2011. "Characterization of fracture properties of asphalt mixtures based on cohesive zone modeling and digital image correlation technique." *Transportation Research Board 2011 Annual Meeting*, Washington, D.C.

Bazant, Z.P. and J. Planas. 1998. *Fracture and size effect in concrete and other quasibrittle materials*. Boca Raton, FL: CRC Press.

Blab, R., and J. T. Harvey. 2002. "Modeling measured 3D tire contact stresses in a viscoelastic FE pavement model." *International Journal of Geomechanics*, *2*, no. 3: 271-290.

Collop, A. C., A. Scarpas, C. Kasbergen, and A. Bondt. 2003. "Development and finite element implementation of stress-dependent elastoviscoplastic constitutive model with damage for asphalt." *Transportation Research Record*, *1832* : 96-104.

Dassault Systemes SIMULIA Ltd. 2008. *ABAQUS. Version 6.8*. Available from wwwl.3ds.com

Duan, K., X. Hu, and F. H. Wittmann. 2006. "Scaling of quasi-brittle fracture: Boundary and size effect." *Mechanics of Materials*, 38: 128-141.

Elseifi, M. A., and I. L. Al-Qadi. 2006. "Modeling of strain energy absorbers for rehabilitated cracked flexible pavements." *Journal of Transportation Engineering*, *131*, no. 9: 653-661.

Elseifi, M. A., I. L. Al-Qadi, and P. J. Yoo. 2006. "Viscoelastic modeling and field validation of flexible pavements." *Journal of Engineering Mechanics, 132*, no. 2: 172-178.

Espinosa, H.D. and P. D. Zavattieri. 2003. "A grain level model for the study of failure initiation and evolution in polycrystalline brittle materials, Part I: Theory and numerical implementation." *Mechanics of Materials, 35*: 333-364.

Geubelle, P. and J. Baylor, J. 1998. "Impact-induced delamination of laminated composites: A 2D simulation." *Composites Part B – Engineering*, 29, no. 5: 589-602.

Haji-Ali, R. and A. Muliana. 2004. "Numerical finite element formulation of the Schapery non-linear viscoelastic material model." *International Journal for Numerical Methods in Engineering, 59*: 25-45.

Huang, C. W., R. K. Abu Al-Rub, R. K., E. A. Masad, and D. N. Little. 2011. "Three-dimensional simulations of asphalt pavement permanent deformation using a nonlinear viscoelastic and viscoplastic model." *Journal of Materials in Civil Engineering, 23,* no. 1: 56-68.

Kim, Y., D. H. Allen, D. H., and D. N. Little. 2007. "Computational constitutive model for predicting nonlinear viscoelastic damage and fracture failure of asphalt concrete mixtures." *International Journal of Geomechanics 7,* no. 2: 102-110.

Kim, Y., D. H. Allen, and G. D. Seidel. 2006. "Damage-induced modeling of elastic-viscoelastic randomly oriented particulate composites." *Journal of Engineering Materials and Technology, 126* : 18-27.

Kim, Y., H. Ban, H., and S. Im. 2011. "Impact of truck loading on design and analysis of asphaltic pavement structures-Phase II." *MATC Final Report No. MATC-UNL 321*, Lincoln, Nebraska.

Kim, H. and W. G. Buttlar. 2009. "Discrete fracture modeling of asphalt concrete." *International Journal of Solids and Structures, 46*: 2593-2604.

Kim, Y. R., J. S. Daniel, and H. Wen, H. 2002. "Fatigue performance evaluation of WestTrack asphalt mixtures using viscoelastic continuum damage approach." *Final Report No. FHWA/NC/2002-004*, North Carolina State University.

Kim, K. W., S. J. Kweon, Y. S. Doh, and T. S. Park. 2003. "Fracture toughness of polymer-modified asphalt concrete at low temperatures." *Canadian Journal of Civil Engineering, 30*: 406-413.

Kim, H., M. P. Wagoner, and W, G. Buttlar. 2008. "Simulation of fracture behavior in asphalt concrete using a heterogeneous cohesive zone discrete element model." *Journal of*

Materials in Civil Engineering, *20*, no. 8: 552-563.

Lai, J. and A. Bakker. 1996. "3-D Schapery representation for non-linear viscoelasticity and finite element implementation." *Computational Mechanics*, *18*: 182-191.

Li, X. and Marasteanu, M. O. (2005). "Cohesive Modeling of Fracture in Asphalt Mixtures at Low Temperatures." *International Journal of Fracture*, 136, 285-308.

Li, X. and M. O. Marasteanu. 2010. "The fracture process zone in asphalt mixture at low temperature." *Engineering Fracture Mechanics*, *77*: 1175-1190.

Marasteanu, M. O., A. Zofka, M. Turos, X. Li, R. Velasques, X. Li, W. Buttlar, G. Paulino, A. Braha, E. Dave, J. Ojo, H. Bahia, C. Williams, J. Bausano, A, Gallistel, and L. McGraw. 2007. "Investigation of low temperature cracking in asphalt pavements: National pooled fund study 776." *Final Report No. MN/RC 2007-43*, Minnesota Department of Transportation.

Masad, E., and N. Somadevan. 2002. "Microstructural finite-element analysis of influence of localized strain distribution of asphalt mix properties." *Journal of Engineering Mechanics*, 128: 1105–1114.

Mobasher, B., M. Mamlouk, and H. Lin. 1997. "Evaluation of crack propagation properties of asphalt mixtures." *Journal of Transportation Engineering*, *123*, no. 5: 405–413.

Mull, M. A., K. Stuart, and A. Yehia. 2002. "Fracture resistance characterization of chemically modified crumb rubber asphalt pavement." *Journal of Materials Science*, 37: 557-566.

Mun, S., M. Guddati, and Y. R. Kim. 2004. "Fatigue cracking mechanisms in asphalt pavements with viscoelastic continuum damage finite element program."0 *Transportation Research Record*, 1896: 96-106.

Schapery, R. A. 1969. "On the Charcaterization of Nonlinear Viscoelastic Materials." *Polymer Engineering and Science*, 9: 295-310.

Seo, Y., Y. R. Kim, and M. W. Witczak. 2002. "Application of the digital image correlation method to mechanical testing of asphalt-aggregate mixtures." *Transportation Research Record, 1789: 162*-172.

Soares, R. F., D. H. Allen, Y. Kim, C. Berthelot, J. B. Soares, J. B., and M. E. Rentschler. 2008. "A computational model for predicting the effect of tire configuration on asphaltic pavement life." *International Journal on Road Materials and Pavement Design*, *9*, no. 2: 271-289.

Song, S. H., G. H. Paulino, and W. G. Buttlar. 2006. "A bilinear cohesive zone model tailored for fracture of asphalt concrete considering viscoelastic bulk material." *Engineering Fracture Mechanics, 73*, no. 18: 2829-2847.

Song, S. H., M. P. Wagoner, and G. H. Paulino. 2008. "δ_{25} crack opening displacement parameter in cohesive zone models: Experiments and simulations in asphalt concrete." *Fatigue and Fracture of Engineering Materials and Structures, 31*: 850-856.

Wagoner, M. P., W. G. Buttlar, and G. H. Paulino. 2005. "Development of a single-edge notched beam test for asphalt concrete mixtures." *Journal of Testing Evaluation*, 33, no. 6: 452–460.

Wagoner, M. P., W. G. Buttlar, and G. H. Paulino. 2005. "Disk-shaped compact tension test for asphalt concrete fracture." *Society for Experimental Mechanics,* 45, no. 3: 270–277.

Yoo, P. J. 2007. "Flexible pavement dynamic responses analysis and validation for various tire configurations." PhD Diss., University of Illinois at Urbana-Champaign.

Zhao, Y. 2002. "Permanent deformation characterization of asphalt concrete using a viscoelasticplastic model." PhD Diss., North Carolina State University.